RADIOMETRY-BASED RANGE PREDICTION FOR MID- AND LONG-WAVE INFRARED IMAGING SYSTEMS

A THESIS SUBMITTED TO
THE GRADUATE SCHOOL OF NATURAL AND APPLIED SCIENCES
OF
MIDDLE EAST TECHNICAL UNIVERSITY

BY

BERK BERKAN TURGUT

IN PARTIAL FULFILLMENT OF THE REQUIREMENTS
FOR
THE DEGREE OF MASTER OF SCIENCE
IN
MICRO AND NANOTECHNOLOGY

SEPTEMBER 2018

Approval of the thesis:

RADIOMETRY-BASED RANGE PREDICTION FOR MID- AND LONG-WAVE INFRARED IMAGING SYSTEMS

submitted by **BERK BERKAN TURGUT** in partial fulfillment of the requirements for the degree of **Master of Science in Micro and Nanotechnology Department, Middle East Technical University** by,

Prof. Dr. Halil Kalıpçılar _____
Dean, Graduate School of **Natural and Applied Sciences**

Prof. Dr. Burcu Akata Kurç _____
Head of Department, **Micro and Nanotechnology**

Assoc. Prof. Dr. Alpan Bek _____
Supervisor, **Physics Dept., METU**

Assist. Prof. Dr. Serdar Kocaman _____
Co-supervisor, **Electrical and Electronics Eng. Dept, METU**

Examining Committee Members:

Prof. Dr. Barış Akaoğlu
Physics Engineering, Ankara University _____

Assoc. Prof. Dr. Alpan Bek
Physics Department, METU _____

Assoc. Prof. Dr. Akın Bacıoğlu
Physics Engineering, Hacettepe University _____

Assoc. Prof. Dr. Serhat Çakır
Physics Department, METU _____

Assoc. Prof. Dr. Özgür Ergül
Electrical and Electronics Engineering Department, METU _____

Date: _____

I hereby declare that all information in this document has been obtained and presented in accordance with academic rules and ethical conduct. I also declare that, as required by these rules and conduct, I have fully cited and referenced all material and results that are not original to this work.

Name, Last Name: BERK BERKAN TURGUT

Signature :

ABSTRACT

RADIOMETRY-BASED RANGE PREDICTION FOR MID- AND LONG-WAVE INFRARED IMAGING SYSTEMS

Turgut, Berk Berkan
M.S., Department of Micro and Nanotechnology
Supervisor : Assoc. Prof. Dr. Alpan Bek
Co-Supervisor : Assist. Prof. Dr. Serdar Kocaman

September 2018, 77 pages

The present study is about the mid- and long-wave infrared imaging systems in which radiometry-based range prediction are performed. In this study, radiometry-based detection, recognition and identification range prediction equation is derived by using an optical design, optomechanical and optoelectronic structure for particular targets, atmospheric conditions, and backgrounds. Analysis of the atmospheric transmittance value for four different atmospheric conditions at mid- and long-wave is performed in detail with help of MODTRAN^{TM} 5 software. Detection, recognition and identification range for land, sea, and air targets is obtained using Johnson criteria. In view of different target types, the effect of the target area on range is examined. Furthermore, the effect of optical aspects of infrared optical systems -aperture and transmittance- and atmospheric conditions on range prediction performance is examined and discussed for both mid- and long-wave bands in this thesis.

This study is designed to provide useful information for forthcoming infrared imaging system designers significantly in their designs targeting infrared search and tracking.

Keywords: Infrared, Range, Radiometry, MODTRAN

ÖZ

ORTA VE UZUN DALGABOYU KIZILÖTESİ GÖRÜNTÜLEME SİSTEMLERİ İÇİN RADYOMETRİ TABANLI MENZİL TAHMİNİ

Turgut, Berk Berkan
Yüksek Lisans, Mikro ve Nanoteknoloji Bölümü
Tez Yöneticisi : Doç. Dr. Alpan Bek
Ortak Tez Yöneticisi : Yrd. Doç. Dr. Serdar Kocaman

Eylül 2018 , 77 sayfa

Bu tez çalışmasında, orta ve uzun dalga boyu kızılötesi görüntüleme sistemleri için radyometri tabanlı menzil tahmini üzerine bir çalışma yapılmıştır. Çalşma esnasında belirli bir senaryo içinde bulunan hedefi, belirli bir atmosferik koşul ve belirli bir arka plan varlığında tasarlanmış bir optik, optomekanik ve optoelektronik sistem ile tespit, teşhis ve tanımlama amaçlı olarak radyometri tabanlı menzil tahmini denklemi ortaya konmuştur. MODTRAN^{TM}5 yazılımı yardımı ile orta ve uzun dalga boyunda dört farklı atmosferik koşul için atmosferik geçirgenlik değerinin analizi detaylı olarak yapılmıştır. Johnson kıstasına göre kara, deniz ve hava hedefleri için tespit, teşhis ve tanımlama menzil değerleri elde edilmiştir. Hedef tipleri birbirlerinden oldukça farkli olabildiği için hedef alanının menzile etkisi incelenmiştir. Buna ek olarak, optik sisteme özel giriş açıklığı ve optk geçirgenlik değerleri ile atmosferik geçirgenlik değerinin menzile olan etkileri iki dalga boyu bandında detaylı olarak incelenmiştir.

Yapılan bu çalışma, kızılötesi görüntüleme sistemi tasarımcıları için gelecekte yapmayı hedefledikleri kızılötesi arama ve takip sisteme tasarımları açısından önemli ve yararlı bilgiler sağlamış olacaktır.

Anahtar Kelimeler: Kızılötesi, Menzil, Radyometri, MODTRAN

To my current and future family

Songül Turgut, Memet Turgut, Özhan Turgut and Zeynep İpek

ACKNOWLEDGMENTS

I would like to express my sincere gratitude to my advisor Assoc. Prof. Dr. Alpan Bek for the continuous his guidance, motivation and patience throughout my thesis study and research. Also I would like to thank Assist. Prof. Dr. Serdar Kocaman for his cooperation in studies.

I am thankful to my unit chief, colleagues, and the staff in TÜBİTAK SAGE, Optical Design Division for their support and friendship as well as increasing the quality of my study with their remarks and recommendations.

I would like to thank all my friends for nice conversations during social activities.

I would like to express my endless thanks to my love Zeynep İpek. Throughout my master's degree studies, my love gave me all motivation and liveliness to complete this study.

Finally, I would like to express my endless thanks and enthusiasm, motivation, and gratitude to my mom (Songül Turgut) dad (Memet Turgut) and brother (Özhan Turgut) and supporting me throughout all my life. Without their love, patience I would not have been able to finish this thesis.

TABLE OF CONTENTS

LIST OF TABLES

TABLES

LIST OF FIGURES

FIGURES

LIST OF ABBREVIATIONS

MWIR	Mid- Wave Infrared
LWIR	Long- Wave Infrared
IRST	Infrared Search and Track
HgCdTe	Mercury Cadmium Telluride
IR	Infrared
EM	Electromagnetic
NIR	Near Infrared
SWIR	Short Wave Infrared
FPA	Focal Plane Array
HWIL	Hardware-in-the-Loop
NEP	Noise Equivalent Power
DRI	Detection, Recognition and Identification
VIS	Visibility
AC	Atmospheric Condition
FOV	Field-of-View
SNR	Singal-to-Niose
E	Irradiance
L	Radiance
I	Radiant Intensity
M_λ	Spectral Exitance
M	Total Exitance
T	Temperature
Φ	Radiant Flux or Power

Ω	Solid Angle
ρ	Absorbance
α	Reflectance
τ	Transmittance
λ	Wavelength
ϵ	Emissivity
km	kilometer
μm	micrometer
f	Focal Length
GUI	Graphical User Interface

CHAPTER 1

INTRODUCTION

1.1 Scope of Thesis

In this thesis, mid- and long-wave infrared imaging systems are analyzed in the sense of radiometry-based range. The aim is to develop a radiometry-based detection, recognition, and identification range performance database with respect to Johnson criteria of infrared imaging systems. In literature, an database for comparing the ranges of mid and long wave infrared imaging systems is lacking. In this work, The effects of the optics, detector, target, background, and atmospheric model parameters on range performance are examined and discussed in oder to provide the missing crucial information in literature. The accurate prediction of the expected range performance is of utmost importance imaging system designers with a purpose of infrared search and tracking.

1.2 Historical Background

The invention of infrared radiation is ascribed to William Herschel who announced his finding in 1800. Herschel is the first to detect radiation beyond the red region of the spectrum, through an increase in the temperature recorded on a thermometer. He used a prism to refract light from the sun. He called this radiation as "Calorific Rays" [1, 2]. The term "**infrared**" was commonly accepted late in 19th century [3].

After the "**infrared**" term, there has been a lot of milestones regarding research in the infrared. Here, significant discoveries which are directly related to this thesis are listed below:

- In 1840, John Herschel created the first thermal image thermograms [4]. These thermograms provide a method to detect radiation in the long- infrared range and to capture creative images of that radiation.
- In 1860, Gustav Kirchhoff formulated the blackbody theorem [5].
- In 1901, Max Planck published the blackbody equation and corresponding theorem [6].
- In 1905-1908, William Coblentz published infrared spectra in units of wavelength (microns) for several chemical compounds in "Investigations of Infra-Red Spectra" [7, 8, 9].
- In 1917, Theodore Case developed the thallous sulfide detector. British scientist built the first infra-red search and track (IRST) device which is capable of detecting on aircraft at a range of one mile (1.6 km) [10, 11].
- In 1929, Kalman Tihanyi invented the infrared-sensitive (night vision) electronic television camera that is used for anti-aircraft defense in Britain [12, 13].
- In 1945, The Zielgerat 1229 "Vampir", first portable infrared device for military applications was developed. [5].
- In 1958, Falcon and Sidewinder missiles were developed using infrared technology [5].
- In 1958, W.D. Lawson discovered IR detection properties of Mercury Cadmium Telluride (HgCdTe) [5].
- In 1965, First IR Handbook; first commercial imagers (Barnes, Agema); U.S. Army's night vision lab formed were developed, and Rachets develops detection, recognition and identification modeling there [5, 14].

The developments in this area are evolving rapidly day-by-day thanks to the advancement in technology. Infrared radiation is used in industrial, scientific, military, law

enforcement, and medical applications. Comprehensive uses for military and civilian applications include target acquisition, surveillance, night vision, homing, and tracking [15]. In this study calculation for range prediction of infrared imaging system used in military applications is explained in detail.

Mohammad et al. [16] have worked on range prediction [16]. The lock-on range of infrared heat seeker missile is studied in their work. An analytical expression form of range is also derived. The "Lambert W function" is used for the range prediction in this work. However, in this work atmospheric attenuation was not modeled in detail. In addition to that, background noise from background temperature fluctuations was not taken into. Only Noise Equivalent Irradiance (NEI) was used for characterization of noise.

Another study on the same topic is by Shahid Baqar [17]. He mentioned lock-on range only as a part of his doctoral thesis. He has obtained an analytical formula of range on that part, but a detail analysis was not performed [17]. His solution was based on "MATLAB^{TM} fzero function" for the range prediction, because range prediction equation doesn't have an exact solution.

1.3 Organization of the Thesis

The remaining part of the thesis consists of five chapters as follows: In Chapter 2, the fundamental information of electromagnetic radiation at the infrared band is given in detail. In Chapter 3, using MODTRAN^{TM} software, atmospheric transmission value of the mid and long wave infrared band at different atmospheric models is investigated in detail. In Chapter 4, how to obtain theoretically range prediction formula using radiometry and range discrimination is discussed in detail. In Chapter 5, calculation and result of radiometry based range prediction formula and the effects of properties of optics, detector, target, background and atmospheric model parameters to range performance is examined in detail. In Chapter 6, conclusion and discussion of this thesis work is provided.

CHAPTER 2

THE ELECTROMAGNETIC RADIATION AT THE INFRARED

The electromagnetic (EM) spectrum is very broad and includes all types of electromagnetic radiation, ranging from Gamma - rays to Radio waves [18]. One significant region of the EM spectrum is infrared (IR) radiation, located between visible and radio waves, as illustrated in the Figure 2.1.

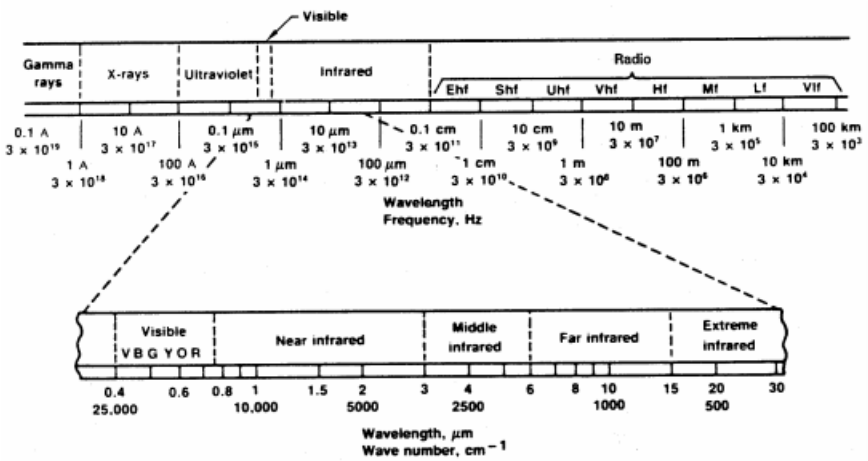

Figure 2.1: Electromagnetic spectrum [18]

IR is discovered experimentally around the year 1800 by Sir Fredick William HERSCHEL [18]. The IR spectrum has five different subregions. These regions are dependent on an association transmittance of atmosphere and wavelength. Some subregions of the IR region have higher atmospheric transmittance, on the other hand, others have less or none at all. Because of this, those regions or wavelength intervals are defined as "atmospheric windows" [20]. IR sensors or detector branches are designed by taking into account atmospheric windows. There are four utmost atmospheric windows of the IR region, known as the Near Infrared Band (NIR), Short

Wave Infrared (SWIR), Mid Wave Infrared (MWIR) and Long Wave Infrared (LWIR) [19] are shown in Figure 2.2. For the fiber optic telecommunication systems, NIR is the most suitable band, whilst SWIR is the best choice for long distance telecommunications such as remote sensing [21, 29]. Hence, MWIR, from 3 to 5 μm, and LWIR, from 8 to 14 μm have many applications both in IR imaging for civil and especially military areas such as, target signature detection, recognition, identification, tracking, searching, and surveillance, etc.[21, 28, 31] . The value of transmittance directly depends on gases in the atmosphere, which include a combination of carbon dioxide (CO_2), water (H_2O), nitrogen (N_2), oxygen (O_2), and ozone (O_3) molecules. These molecules affect diverse IR bands. For example, while (H_2O) is effective in the NIR and LWIR bands, ozone (O_3) and (CO_2) are effective in the MWIR band. The absorption occurring due to their vibrations attenuates the transmission of IR radiation. In addition to absorption, the scattering that occurs from particles in the atmosphere also attenuates transmission [20].

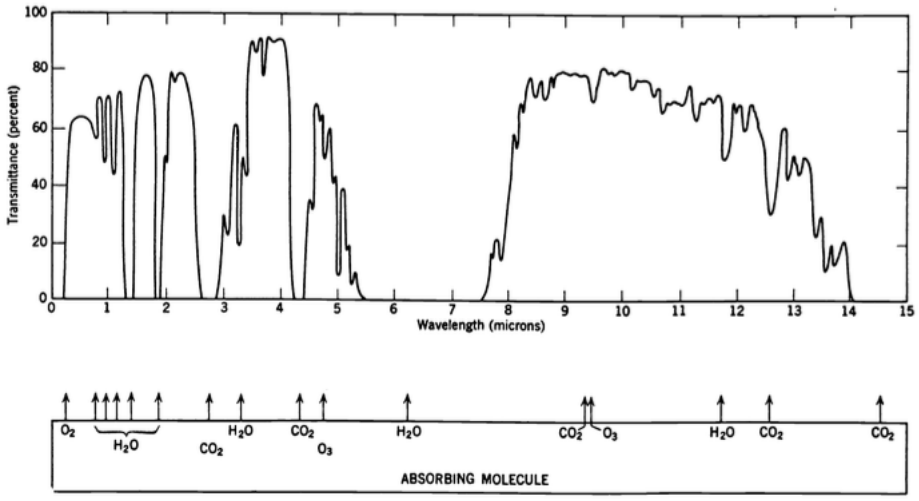

Figure 2.2: Atmospheric transmittance in infrared region [20]

The fundamental difference between visible, which can be observed, and infrared or thermal radiation, is that visible radiation requires reflection and external source radiance, whereas IR radiation does not. All objects have above absolute zero (i.e., 0 K = -273.15 °C) defined as "Self Radiation" which is a physical property [19]. All objects made of atoms, emit infrared or thermal radiation due to the vibration of those atoms. That kind of radiation is directly related to properties of the object such as temperature, surface characteristics (i.e., emissivity, reflectivity) and etc [21]. Ob-

jects with higher temperatures emit more radiation than those with low temperature. Smooth surfaces emit lower radiation as compared to objects with rough surfaces. These surfaces with very high temperatures get red-hot and the thermal radiations can be noticed with respect to sight. For instance, the sun, example of object, which is almost 6000 K is seen by humans that emits IR radiation [21]. But even at calm or average in amount temperature, the radiation can be distinguished as heat but not in visible region. IR radiation of the objects with below a certain temperature cannot be felt by the humans but that radiation still exists. In fact, at low temperatures such as room temperature (i.e 293.15 Kelvin), the objects have IR radiation with different wavelengths and severity [21].

IR radiation is invisible to naked eye. Infrared imaging systems are often used to make this radiation visible and form images of objects under all conditions and any time. Infrared imaging system depends on the interaction of several subsystems which are shown in Figure 2.3.

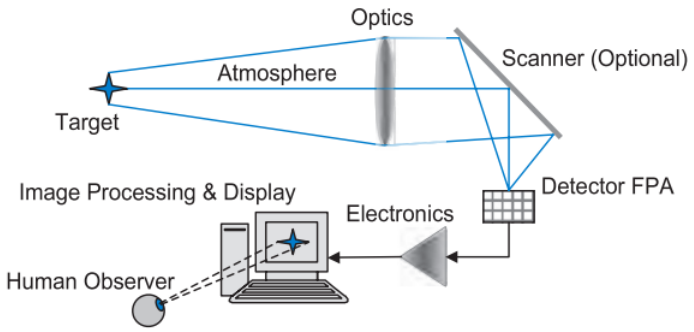

Figure 2.3: Infrared imaging system concepts [21]

Infrared imaging systems have three main subsystems: optical system, atmosphere, and detector. Subsystems such as electronics and imaging processing support the main subsystem. Optical system, in short optics, is used to collect and divert the optical path by reflecting and refracting the infrared radiation from the objects and focus all radiation on the Detector Focal Plane Array (FPA)[21, 30]. The optic systems consist of a combination of diverse types optical components such as lens, prism, and mirror. The infrared detector is a sensor, or transducer, that is used to convert the signal proportional to the total infrared radiation incident on the IR detector FPA surface into an electrical signal and electronics amplifies that to a useful level [21]. After image processing the object can be seen by the naked eye through a display.

Table 2.1: Radiometric quantities and units

Radiometric Quantity	**Symbol**	**Unit**
Irradiance	E	W\cm^2
Radiance	L	W\cm^{2}sr
Radiant Intensity	I	W\sr
Spectral Exitance	M_λ	W\cm$^2\mu$m
Total Exitance	M	W\cm^2
Radiance Temperature	T	K
Radiant Flux or Power	Φ	W
Solid Angle	Ω	sr

Any object emits IR radiation that can be given in assorted radiometric quantities. The term radiometry is the science that handles measuring IR radiation with regard to its power, spectral characteristics, temperature, and other parameters according to source location and detector configuration. It means that radiometry is a quantitative understanding of flux transfer or power between a source and a sensor. Radiometric quantities and their units are essential to accomplish radiometry based calculations which is given Table 2.1 [21].

The quantities, exitance (M), radiant intensity (I), and radiance (L) of an object depict the power emitted at all frequencies from an object surface, whilst irradiance (E) represent the power at all frequencies incident upon a surface. These quantities are demonstrated in Figure 2.4.

Planck's radiation law is discovered by Max Planck that explained how to calculate the radiometric quantities [6]. This law is also defined as the blackbody equation. It is a term which is used to describe absorbing all incoming radiation and it is also perfect radiator according to Kirchhoff's law which is also called thermal equilibrium that is the total incident radiation is equal to the sum of absorbed, reflected and transmitted part of incident radiation after interacts with an object [18]. It can be formulated in Equation 2.1 [18] and illustrated in Figure 2.5.

$$\alpha + \rho + \tau = 1 \tag{2.1}$$

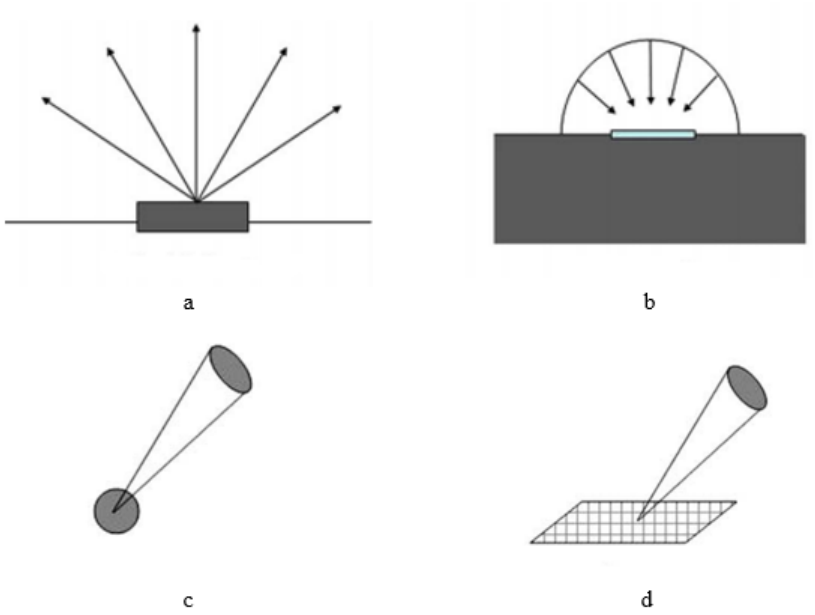

Figure 2.4: Radiometric quantities: a. radiant exitance b. radiant incidence c. radiant intensity d. radiance [22]

Here, α stands for reflectance, ρ denotes the absorbance and τ is the transmittance. These are wavelength dependent. For the blackbody, which is good absorber, is also good emitter ($\alpha = \epsilon$) [23], $\alpha = \epsilon = 1$, $\rho = 0$ and $\tau = 0$. In other words, it does not transmit or reflect any part of the incident radiation [23].

Spectral exitance of blackbody, which is wavelength and temperature dependent, can be specified with using Planck's radiation law which is given Equation 2.2 [23].

$$M_\lambda = \frac{2\pi hc^2}{\lambda^5} \frac{1}{e^{\frac{hc}{\lambda kT}} - 1} \tag{2.2}$$

Here, h is the Planck's, and k is the Boltzman's constant: T is the temperature, c is the speed of light and λ is the wavelength. The spectral exitance of a blackbody for the different temperature values from 300 to 1000 K with respect to wavelength results with using Equation 2.2 are shown Figure 2.6.

As seen in Figure 2.6, if the temperature is increased, the spectral radiant exitance also increased for the all wavelength, because of this, each individual result curve for each temperature never crosses each other. Furthermore, the peak value of the

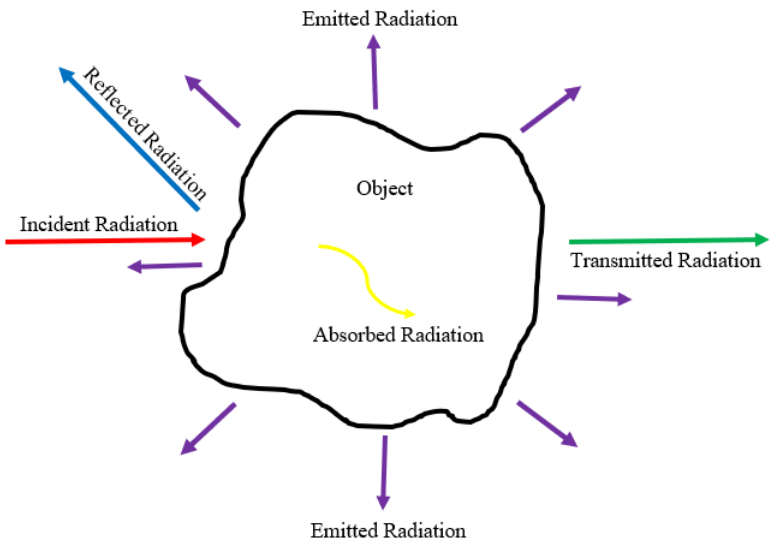

Figure 2.5: Schematic demonstration of Kirchhoff's Law

spectral radiant exitance wavelength is shifted to shorter wavelengths. At specific temperature, for instance 300 K, total spectral radiant exitance can be obtained with the integrating in all wavelength that is given in Equation 2.3 [23].

$$M = \int_0^\infty \frac{2\pi hc^2}{\lambda^5} \frac{1}{e^{\frac{hc}{\lambda kT}} - 1} d\lambda \tag{2.3}$$

Radiance is derived with using total radiant exitance as expressed in Equation 2.4 [23].

$$M = \frac{\Phi}{dA} = \int L d\Omega \tag{2.4}$$

Here, $d\Omega$ denotes solid angle. In the 3-D geometry, it is defined as area on the surface of a sphere (A) divided by square of the radius (r) written in Equation 2.5 [23] and illustrated in Figure 2.7 [21]. This is measured in steradians and dimensionless.

$$\Omega = \frac{A}{r^2} \tag{2.5}$$

If solid angular subtense of any surface of interest is desired, solid angle can be written in Equation 2.6a with differential form. Using the spherical coordinate, which

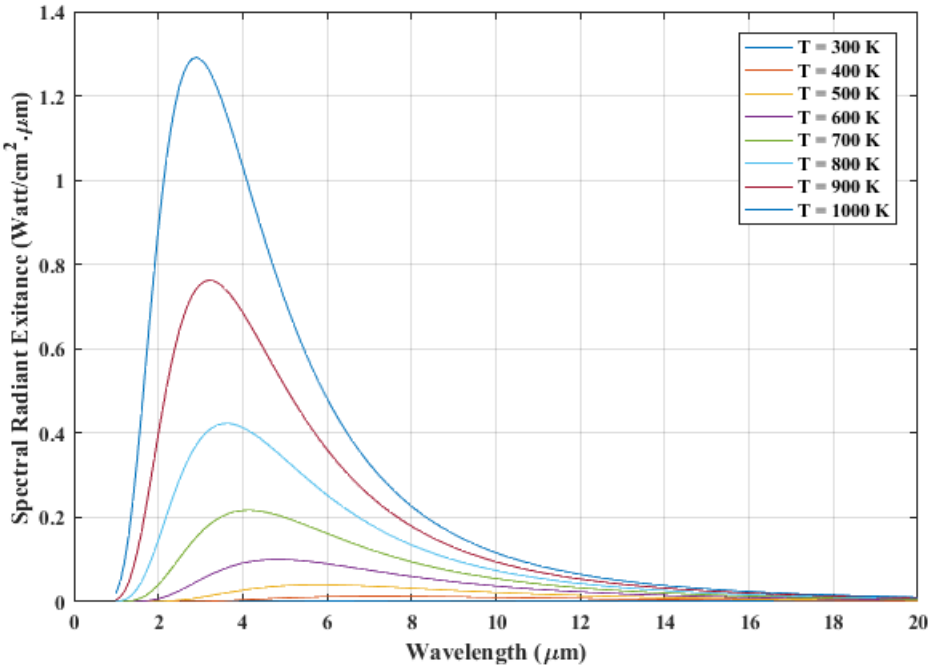

Figure 2.6: Spectral exitance of blackbody

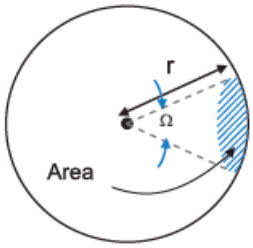

Figure 2.7: Solid angle

is given in Figure 2.8 and dA = r^2 cosθ sinθ dθ dϕ, and inserting in Equation 2.4, radiance should be obtained easily (Equation 2.6c) but if the source is Lambertian whose radiance is independent of view angle. Blackbody is the best example for the Lambertian source which is the same amount of radiance in all direction, or in solid angle [21].

$$d\Omega = \frac{dA}{r^2} \tag{2.6a}$$

$$M = \int L d\Omega = L \int_0^{\frac{\pi}{2}} cos(\theta) sin(\theta) d\theta \int_0^{2\pi} d\phi = \pi L \tag{2.6b}$$

$$L = \frac{M}{\pi} \tag{2.6c}$$

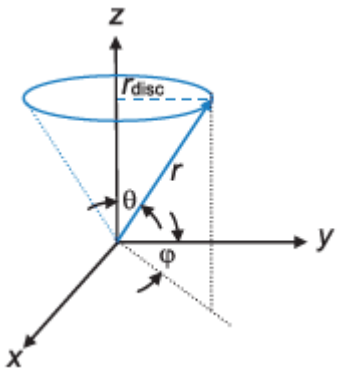

Figure 2.8: Spherical coordinate system [21]

All formulas and information are explained for the ideal source like a blackbody, but in the real world or nature, object or source does not act like ideal one. In fact, perfect blackbody, which would have an emissivity value is one i.e $\epsilon = 1$, the source also does not exist. However, any real object or source would have an emissivity value of less than one i.e $\epsilon < 1$ which is called or defined graybody. Both types of source or object's emissivity are independent of wavelength and can be constant but a selective object or source emissivity is an explicit function of λ [24]. All diverse types of emissivity is showed in Figure 2.9.

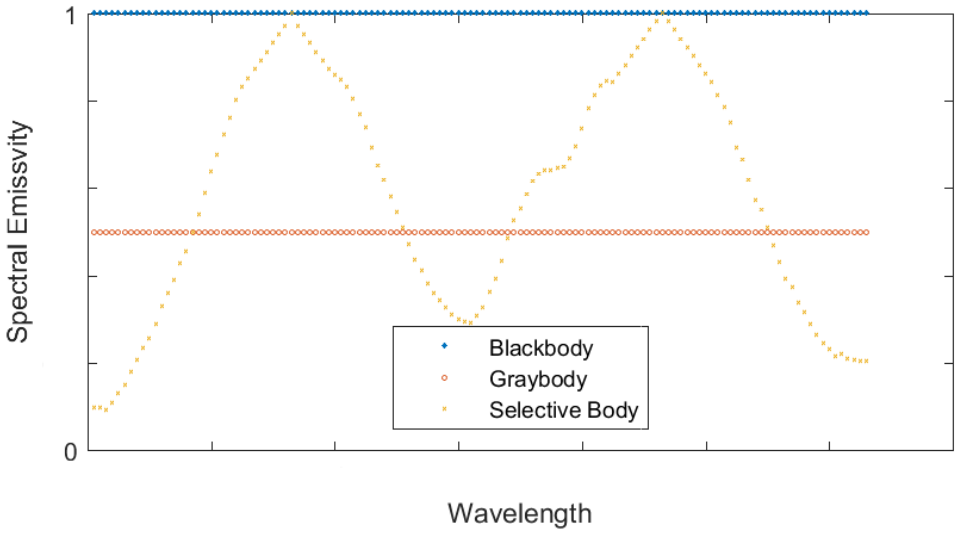

Figure 2.9: Diverse types of emissivity [18]

By the definition of the blackbody, emissivity is divided by the spectral exitance of a real object or source to that of a perfect blackbody at the specific temperature which is expressed in Equation 2.7a [23]. Using Equation 2.7a, spectral or total exitance of real can be obtained in Equation 2.7b, Equation 2.7c and 2.7d [23].

$$\epsilon(\lambda) = \frac{M_{source}(\lambda)}{M_{blackbody}(\lambda)} \tag{2.7a}$$

$$M_{source}(\lambda) = \epsilon(\lambda) M_{blackbody}(\lambda) \tag{2.7b}$$

$$M_{source}(\lambda) = \epsilon(\lambda) \frac{2\pi hc^2}{\lambda^5} \frac{1}{e^{\frac{hc}{\lambda kT}} - 1} \tag{2.7c}$$

$$M_{source} = \int_0^\infty \epsilon(\lambda) \frac{2\pi hc^2}{\lambda^5} \frac{1}{e^{\frac{hc}{\lambda kT}} - 1} d\lambda \tag{2.7d}$$

In this thesis work, spectral exitance, M_λ [W\cm$^2\mu$m], total exitance, M [W\cm^2] and especially radiance, L [W\cm^{2}sr] are used for all calculation.

Next chapter gives the information about the atmospheric transmittance of the mid- and long-wave infrared band at four different atmospheric conditions.

CHAPTER 3

ATMOSPHERIC TRANSMISSION OF MID-AND LONG-WAVE INFRARED BAND

Every infrared imaging system is extremely influenced by atmospheric situations such as clear sky, rain or fog etc. The transmission of infrared radiance through the atmosphere is attenuated. In the literature, MODTRAN^{TM} is the most up-to-date and common software for modeling atmospheric transmittance [23]. As a result, in this thesis, the MODTRAN^{TM} 5.3.2.1 (MODTRAN^{TM}5) software is used to obtain transmittance value for the various atmosphere models at mid-wave and long-wave spectral band. In this work, the mid-wave is defined between 3.6 and 4.9, while long-wave is from 7.7 to 9.3. To calculate the transmission value, MODTRAN^{TM}5 need many input data. In addition to these, for the target/infrared imaging system simulation, information regarding range and altitudes is required. In this way, by working MODTRAN^{TM}5 a few times the transmittance value for the various atmospheric model, constant altitude and ranges from target to infrared imaging system are calculated and stored in an Excel spreadsheet in terms of wavenumber or wavelength.

Table 3.1: Four atmospheric conditions

Parameters	**Variety**
Atmospheric Model	Mid – Latitude Summer
Aerosol Model	No Aerosol or Clouds
	Rural - Vis 23 km
	Rural - Vis 5 km
Seasonal	Spring – Summer
Cloud/Rain Aerosol Extension	No
	Cumulus Clouds: base = 0.066 km, top = 3.0 km
	Rain Rate = 2 mm/hr

MODTRAN^{TM}5 provides six different standard model atmospheres and also user defined model. One of the atmospheric model is the 1976 U.S. Standard Atmosphere which is from a standard atmosphere model but the others are five seasonal models which are Tropicals (15 N latitude), Mid-Latitude Summer and Winter (45 N latitude, July and January, respectively), Sub-Artic Summer and Winter (60 N latitude, July and January, respectively). These model is composed by data from a broad diversity of informant to act for usual seasonal and latitude in atmospheric model. In addition to these model, user defined Model Atmosphere allows the user define their own atmospheric profiles. The model atmospheres describe a 34 layer atmosphere and includes the following data for each layer: altitude, pressure, temperature, water vapor density, and layer concentration of ozone, methane, nitrous oxide, carbon monoxide, carbon dioxide, oxygen, nitric oxide, sulphur dioxide, nitrogen dioxide, and ammonia [25].

For the aerosol model that is used for the 0-2 km calculations, MODTRAN^{TM}5 provides twelve various aerosol model which are Aerosol Free Clouds, No Aerosol Attenuation, Rural - VIS=23 km, Rural - VIS=5 km, Navy Maritime, Maritime - VIS=23 km, Urban -VIS=5 km, Tropospheric - VIS=50 km, User Defined - VIS=23 km, Fog advection - VIS=0.5 km, Fog advection - VIS=0.2 km and Desert Extinction [25].

Furthermore, seasonal parameter in MODTRAN^{TM}5 provides the two options which

are Spring−Summer and Fall−Winter. This parameter is depend on the aerosol model. For instance if the region is a tropical, spring-summer should be generally used, on the other hand if the region is subarctic, fall-winter should be used due to depend on the amount of tropopause [25].

Cloud/Rain Aerosol option permits use of a sequences of cloud extinction models such as, No Clouds or Rain, Cumulus, Altostratus, Stratus, Stratus/Strato and Nimbostratus Clouds and 2.0, 5.0 12.5, 25.0 as well as 75.0 mm/hr Rain that are provided as part of MODTRAN^{TM}5 [25].

With this information regarding MODTRAN^{TM}5, four different atmospheric models are chosen for this thesis and main input parameters are given in Table 3.1. However, any number of atmospheric model and other information can be calculated and saved in the same Excel spreadsheet.

Atmospheric transmittance value is obtained by using MODTRAN^{TM}5 in Mid- and Long-Wave infrared spectral band for the each atmospheric condition given in Table 3.2.

First, atmosphere transmittance at the mid-wave infrared band for the atmospheric condition given in Table 3.2 is investigated. The distance between the infrared imaging system and target is constantly alter throughout the system-target engagement simulation. Atmospheric transmittance value directly depends on the range. Range values of 1, 5, 10 and 20 km are taken in this work at constant altitude to better understand the effect of range. Furthermore, theoretically atmospheric transmittance is calculated in Equation 3.1 [23]. This equation also known as Beer-Lambert law

$$\tau_{atmosphere} = e^{-\sigma R}. \tag{3.1}$$

All result are calculated with using MODTRAN^{TM} 5 software at mid-wave spectral band and long-wave for the atmospheric model given in Table 3.2a − 3.2d with regard to various ranges: R = 1, 5, 10, and 20 km at constant altitude illustrated in Figure 3.1 − 3.4 and Figure 3.5 − 3.8 respectively.

Table 3.2: Atmospheric conditions for mid-wave and long-wave spectral band

Parameters	**Variety**
Atmospheric Model	Mid – Latitude Summer
Aerosol Model	No Aerosol or Clouds
Seasonal	Spring – Summer
Cloud/Rain Aerosol Extension	No

(a) First atmospheric condition

Parameters	**Variety**
Atmospheric Model	Mid – Latitude Summer
Aerosol Model	Rural - VIS 23 km
Seasonal	Spring – Summer
Cloud/Rain Aerosol Extension	No

(b) Second atmospheric condition

Parameters	**Variety**
Atmospheric Model	Mid – Latitude Summer
Aerosol Model	Rural - VIS 5 km
Seasonal	Spring – Summer
Cloud/Rain Aerosol Extension	No

(c) Third atmospheric condition

Parameters	**Variety**
Atmospheric Model	Mid – Latitude Summer
Aerosol Model	Rural - VIS 23 km
Seasonal	Spring – Summer
Cloud/Rain Aerosol Extension	Cumulus Clouds:
	Rain Rate = 2 mm/hr

(d) Fourth atmospheric condition

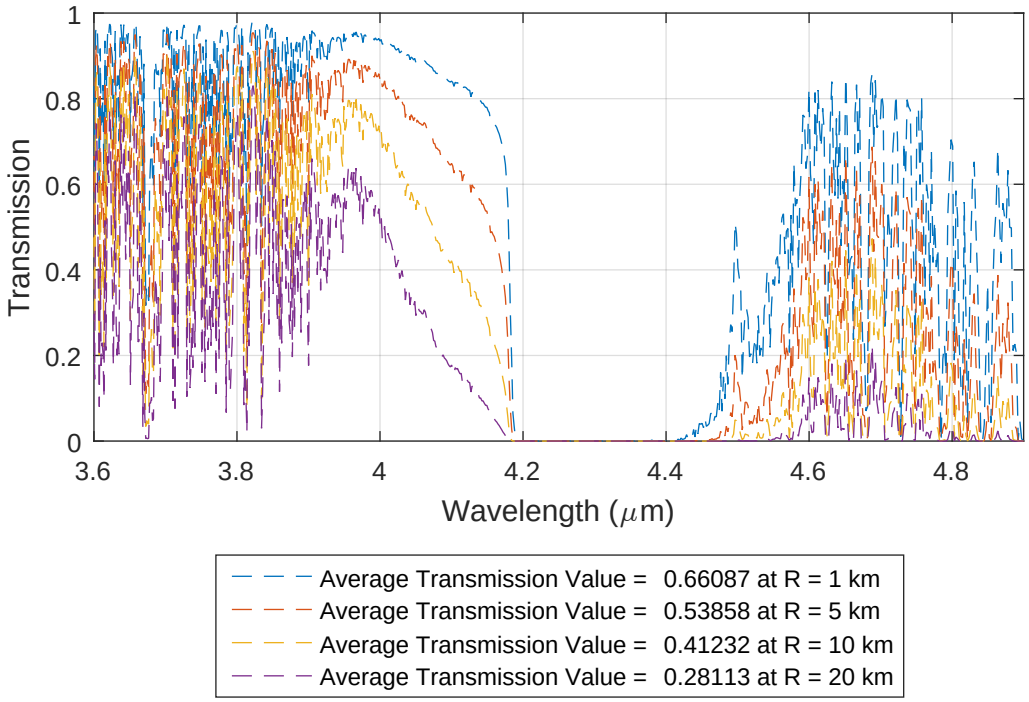

Figure 3.1: MWIR - Atmospheric condition 1

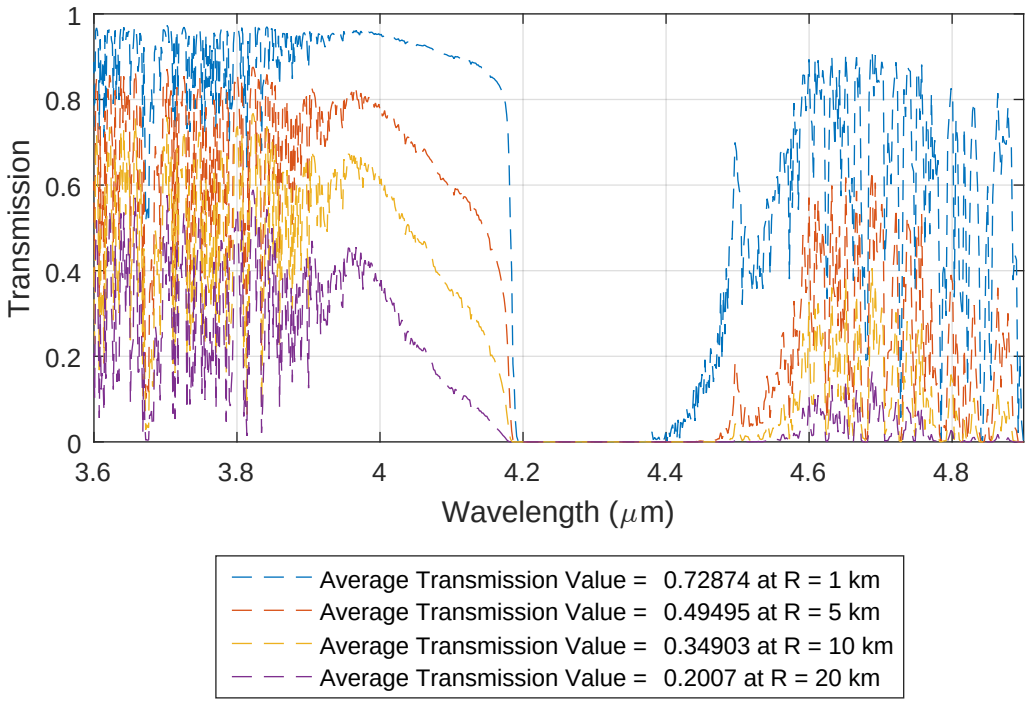

Figure 3.2: MWIR - Atmospheric condition 2

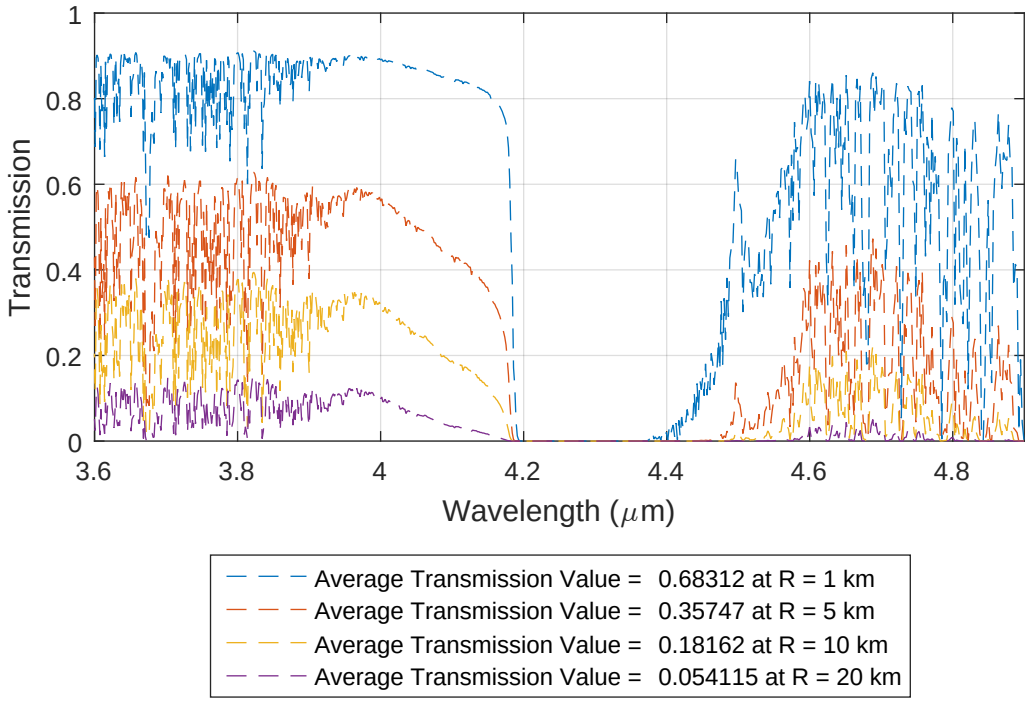

Figure 3.3: MWIR - Atmospheric condition 3

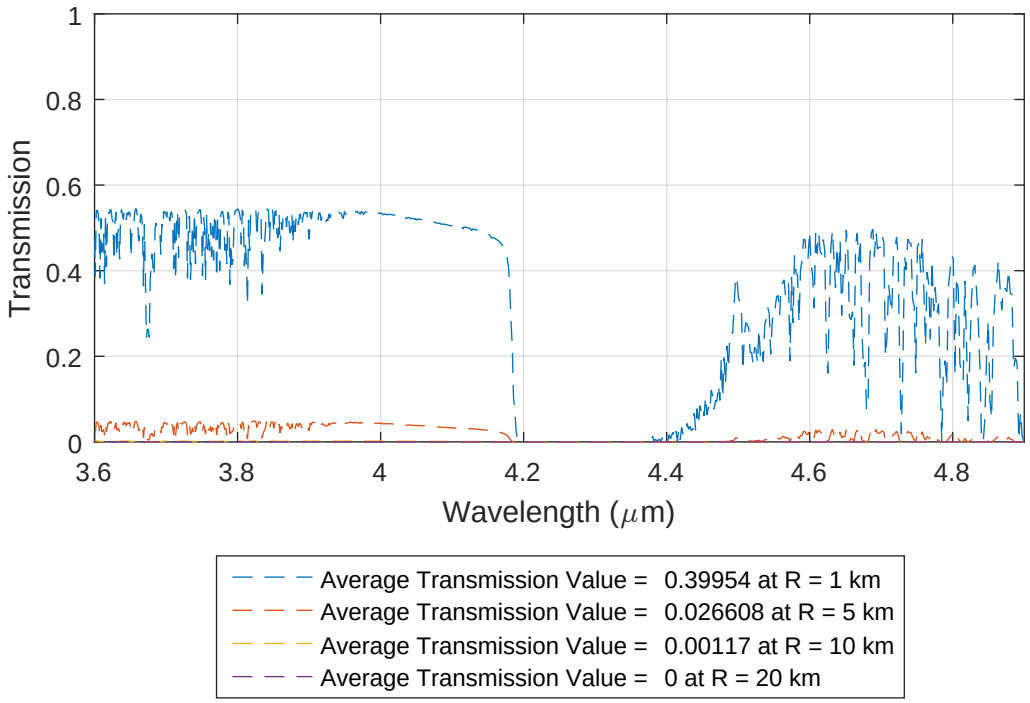

Figure 3.4: MWIR - Atmospheric condition 4

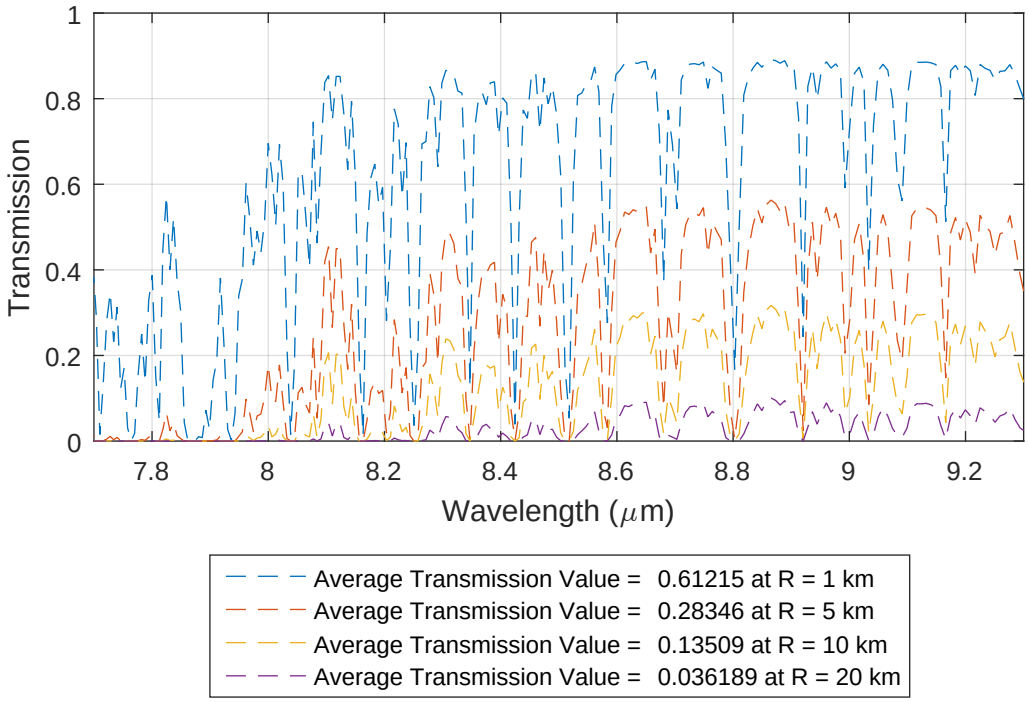

Figure 3.5: LWIR - Atmospheric condition 1

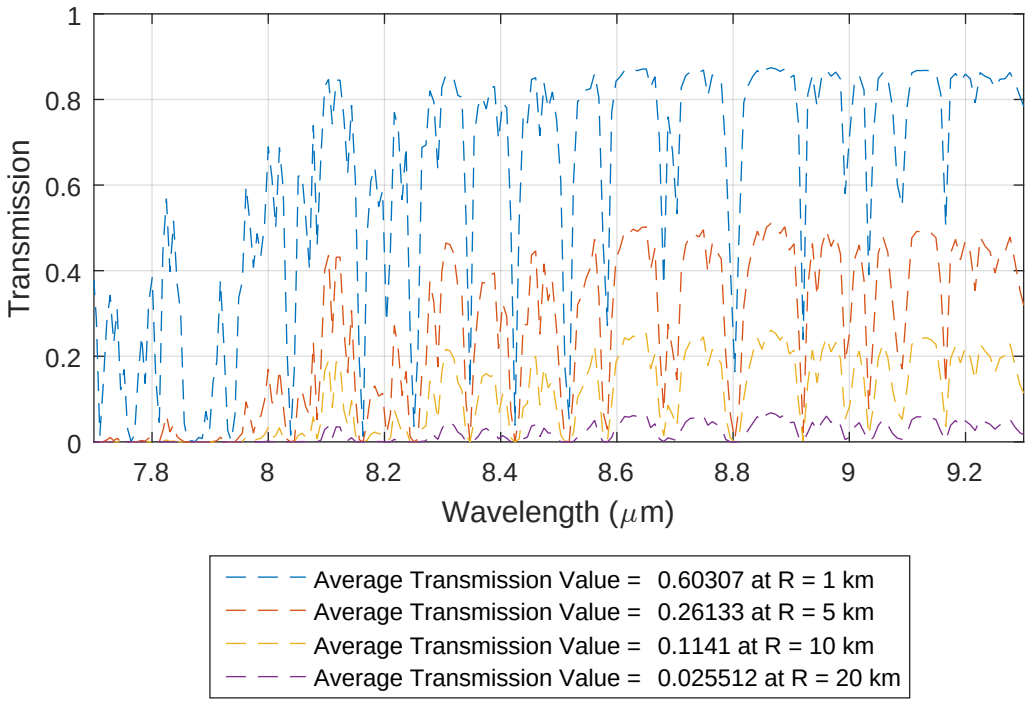

Figure 3.6: LWIR - Atmospheric condition 2

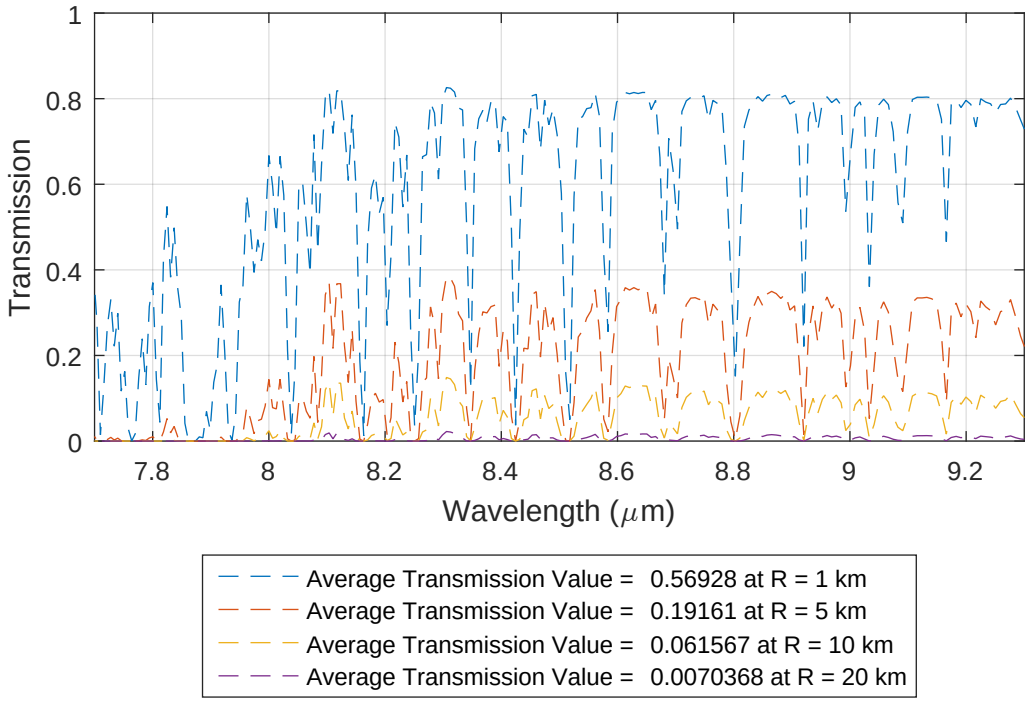

Figure 3.7: LWIR - Atmospheric condition 3

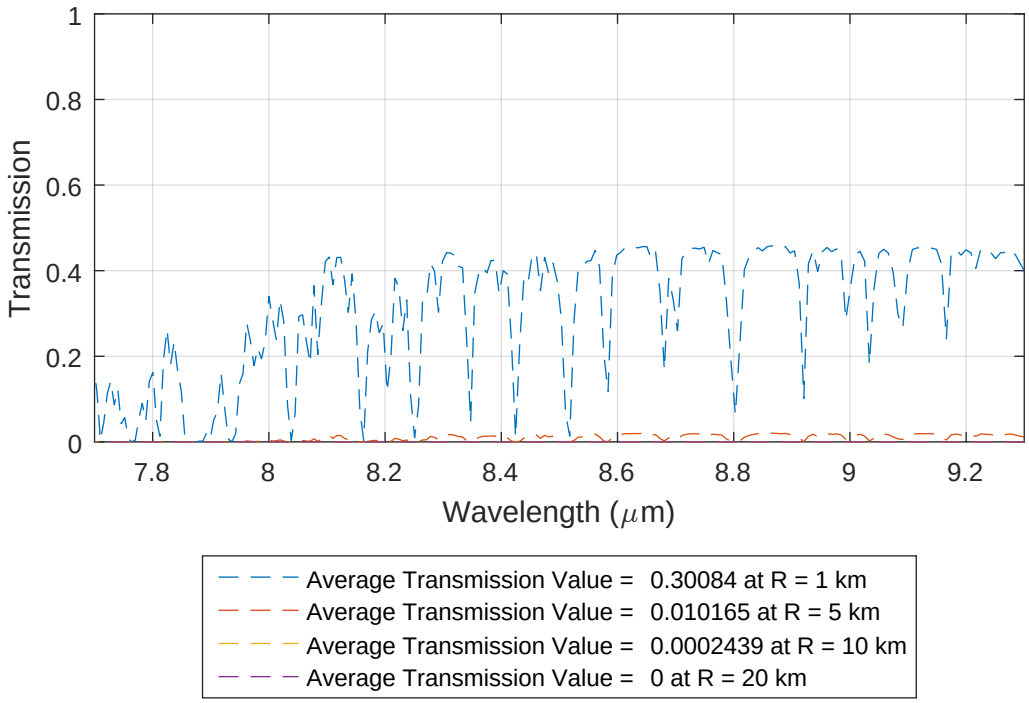

Figure 3.8: LWIR - Atmospheric condition 4

According to all results of four different atmospheric conditions at both spectral bands used in this thesis, the average transmittance values which are calculated without zero values are summarized and given in Table 3.3. As range increases, the average transmittance decreases for each atmospheric model at both spectral bands as seen at Table 3.3. In these atmospheric conditions, MWIR band is higher than LWIR band with regard to atmospheric transmittance. Once the outcomes are investigated, the rainy atmosphere is more likely to affect the transmittance. Also, the transmittance is inversely proportional to the diameter of raindrops and amount of rain such as 2 mm/hr used in this study. Furthermore, the range is an utmost critical parameter for atmospheric transmittance. In fact, as some range value at some atmospheric condition, the transmittance value is zero. For instance, the range is 20 km at the atmospheric condition as given in Table 3.2d , the transmittance is zero for both spectral bands. For this reason, no matter how good the infrared imaging system is, it can not successfully perform because it does not detect the sufficient amount of radiance emitted from the target due to atmospheric transmittance value. Eventually, atmospheric transmittance is extremely significant for the infrared imaging systems.

Next chapter provides methods to obtain radiometry-based range prediction equation and range discrimination.

Table 3.3: Average atmospheric transmittance values

Range (km)	**AC* 1**	**AC 2**	**AC 3**	**AC 4**
1	0.66087	0.72874	0.68312	0.39954
5	0.53858	0.49495	0.35747	0.026608
10	0.41232	0.34903	0.18162	0.00117
20	0.28113	0.2007	0.054115	0.0

(a) Mid- wave spectral band

Range (km)	**AC* 1**	**AC 2**	**AC 3**	**AC 4**
1	0.61215	0.60307	0.56928	0.30084
5	0.28346	0.26133	0.19161	0.010165
10	0.13509	0.11410	0.06156	0.000243
20	0.03618	0.02551	0.007036	0.0

(b) Long- wave spectral band

*AC: Atmospheric Condition

CHAPTER 4

RADIOMETRY-BASED RANGE PREDICTION

4.1 Introduction

Range prediction is a significant part of the infrared imaging system at military applications. IR range prediction computer-based calculation contributes a very cost-effective means to analyses a broad series of scenarios. The objective of this chapter is to give an explanation of the factors influencing IR signature of a scene and obtaining theoretically range prediction formula. Target and background are the main significant steps in the development of IR signature model. Furthermore, atmospheric transmission, detector, and optics are also part of the IR signature model. Range prediction formula is obtained with using radiometry power transfer concepts and the IR signature model.

4.2 Background IR Signature Model

In an IR scene, the background may be made up of one consistent background or mixture of various sub-backgrounds which can be the sky, desert, concrete, forestry etc. In this work, the background is uniform such as desert, meaning constant emissivity value ,i.e independent of wavelength, but less than one, so it is defined as a type of gray-body.

To model IR background signature model needs some input parameters and information: the temperature, emissivity, area of background, and range of the background from the detector.

4.2.1 Radiance of Background in IR Signature Model

Background's IR radiation especially depends on it's temperature and emissivity. Using the Planck's law equation as given in Chapter 2 as Equation 2.2 and 2.6c, the background radiance can be calculated for specified temperature and emissivity value. The total spectral radiance of background, over detector band, can be obtained in Equation 4.1

$$L_{bckgrnd} = \frac{1}{\pi} \int_{\lambda_{cut-on}}^{\lambda_{cut-off}} (\epsilon_{bckgrnd})(\frac{2\pi hc^2}{\lambda^5} \frac{1}{e^{\frac{hc}{\lambda k T_{bckgrnd}}} - 1}) d\lambda. \tag{4.1}$$

where, $L_{bckgrnd}$ is the radiance of the background, $T_{bckgrnd}$ is the temperature of the background, $\epsilon_{bckgrnd}$ is emissivity of the background material, λ_{cut-on} is the cut-on wavelength value of detector, $\lambda_{cut-off}$ is the cut-off wavelength value of detector.

If the background consists of a combination of diverse sub-background, each sub-background radiance can be calculated separately. The total spectral radiance of background should be obtained by collecting each sub-background radiance. The Figure 4.1 shows one example of multiple background.

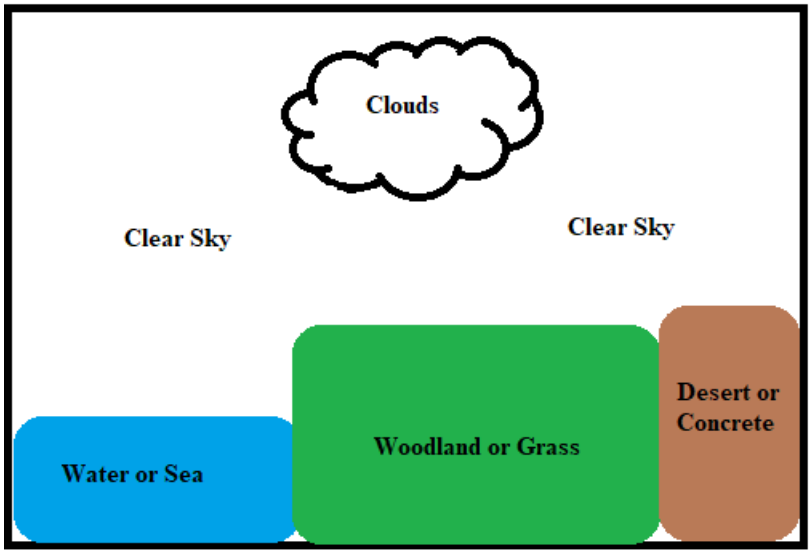

Figure 4.1: Schematic illustration of multiple background

4.3 Target IR Signature Model

For the military application, in an IR scene may include many different types of target such as tanks, aircraft, ships, leaguer, helicopter, military satellite communication area, etc. However, target type directly depends on the background scene. In fact, if the background IR scene consists of only water, target IR scene include quite likely ships. These targets comprises various diverse materials which contain warm and hot surface. Engine of the any target is significant example of hot surface.

To model IR target signature model requires some input parameters and information of each target or sub-target: the temperature, emissivity, area of background, and range of the background from the detector.

4.3.1 Radiance of Target in IR Signature Model

Assuming that target is defined as gray-body and also Lambertian source, target's IR radiation especially depends on its temperature and emissivity. Thanks to Planck's law equation which is given in Chapter 2 as Equation 2.2 and 2.6c, and knowing temperature as well as emissivity value of target, its radiance can be calculated. The total spectral radiance of target, over detector band, can be obtained in Equation 4.2

$$L_{trgtt} = \frac{1}{\pi}\int_{\lambda_{cut-on}}^{\lambda_{cut-off}} (\epsilon_{trgt})(\frac{2\pi hc^2}{\lambda^5}\frac{1}{e^{\frac{hc}{\lambda k T_{trgt}}}-1})d\lambda. \tag{4.2}$$

where, L_{trgt} is the radiance of the target, T_{trgt} is the temperature of the target, ϵ_{trgt} is emissivity of the target material, λ_{cut-on} is the cut-on wavelength value of detector, $\lambda_{cut-off}$ is the cut-off wavelength value of detector.

For the multiple or sub-target, the radiance of each is to be calculated independently. The different types of the target are illustrated in Figure 4.2.

Figure 4.2: The different types of the target: a. and b. land, c. and d. sea, e. and f. air [26]

4.4 Atmosphere IR Signature Model

All IR model is sensitive to atmosphere. Radiance and transmission value are attenuated due to atmosphere. Each different weather conditions such as rain, fog, clear sky, haze, snow and etc. have a different and significant atmospheric effect at IR model. To calculate transmittance of IR atmosphere required some input parameters and information for desired spectral band: weather condition and model, altitude, and path types such as horizontal or slant and etc. In chapter 3, this issue is investigated in detail.

4.4.1 Atmospheric Transmittance in IR Signature Model

Atmospheric transmittance for desired spectral band and atmospheric model value can be obtained in Equation 4.3

$$\tau_{atm} = e^{-\sigma R}. \tag{4.3}$$

Here, σ is the atmospheric attenuation coefficient, τ_{atm} is the atmospheric transmittance, and R is the slant range between target and the sensor or detector.

4.5 IR Detector and Optic Model

The IR detector or optic spectral include perchance any waveband from 1 to 15 μm. The infrared imaging system which combines detector and optic is designed which could depict the whole scene inside its field-of-view (FOV) as a matrix of the pixel. The infrared imaging system is designed with using 640x512 pixel detector. On the other hand, pixel detector can be reduced to less than 640x512, such as 256x256, 128x128 or can be increased to more than 640x512, such as 1024x1024. Pixel detector represent resolution of detector. Characteristic properties of optic, such as FOV, solid angle, transmission of optic, diameter are also significant to design the infrared imaging system.

Signal-to -noise ratio (SNR), focal length (f), transmittance of optic τ_{opt}, diameter of optic, detector pixel size, cut-on and cut-off wavelength of detector and also some noise features of detector are required for IR imaging system.

4.6 Range Prediction in IR Signature Model

Radiometry is a notion that seeks to quantitatively understand the transfer radiant flux or power emitted from a source through the atmosphere and optic elements. The utmost question in the concept of radiometry is how much power emitted from a target or source is gathered by infrared detector. The range prediction can be estimated by

the amount of power falling in the infrared detector. Fundamental and general power or flux transfer is illustrated in Figure 4.3. Par-axial approximation is used in this thesis for the simplification.

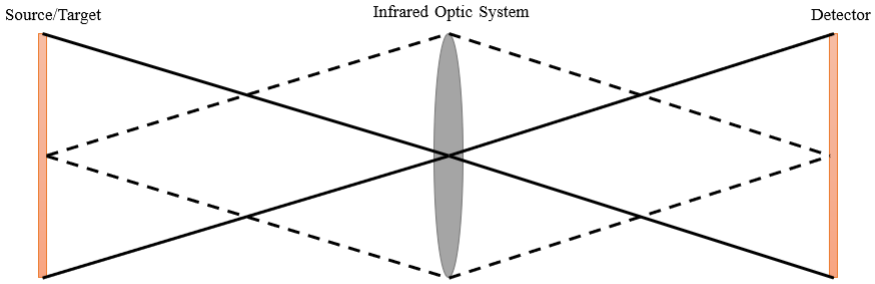

Figure 4.3: Schematic illustration of power transfer in radiometry

Figure 4.4 illustrates an example of a scenario in which three targets (land, sea and air) are given is used for the range prediction in this thesis. These targets are at the same distance from the detector. Target and background radiance collected at the detector in IR signature scenario are computed using example illustrated in Figure 4.4. Before the calculation, it is necessary to define the area of the image plane, or IR model scene, as captured by imaging system is the projected area of the detector as given Equation 4.4. If the target distance from the detector is not same as image distance from the target, which means the target is the distance between image plane and detector, exposed area of the target as projected on image plane must be calculated. Nevertheless, in this work the target distance and image plane from the detector are the same. To better understand regarding the area of target, background and image plane, schematic illustration is given Figure 4.5. According to Figure 4.5, background area is calculated as given Equation 4.5

$$A_{imgpln} = (\frac{ppR}{f})^2. \tag{4.4}$$

Here, pp is the pixel pitch of detector, f is the focal length of imaging system, R is the slant range between image plane and the detector.

$$A_{bckgrnd} = A_{imgpln} - A_{trgt}. \tag{4.5}$$

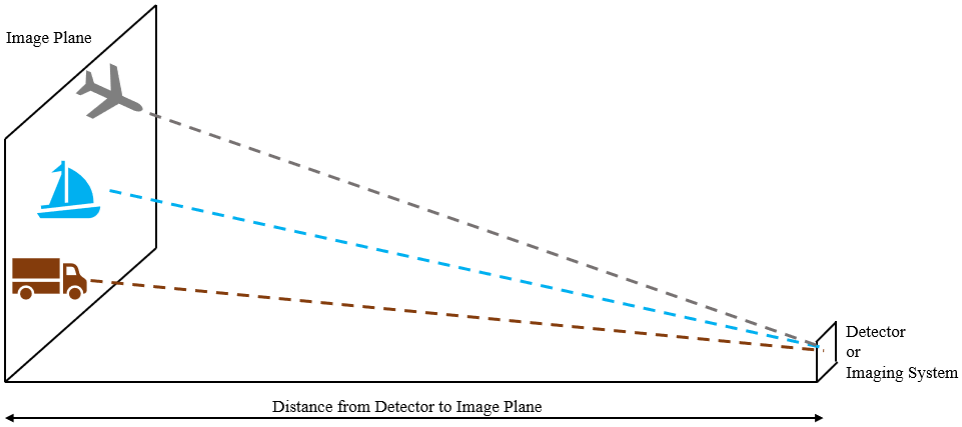

Figure 4.4: Schematic illustration of scenario

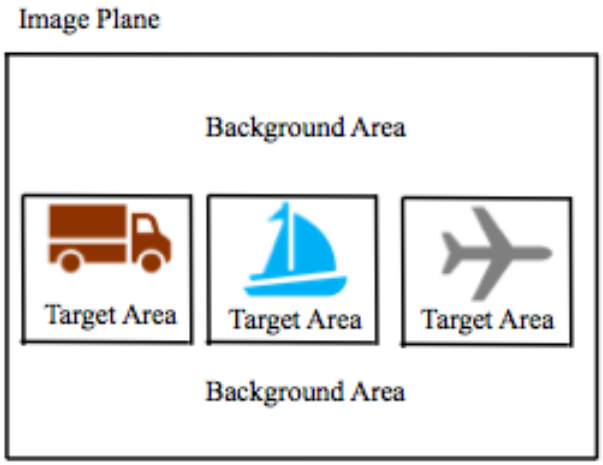

Figure 4.5: Schematic illustration of target, background and image area

Due to solid angle of imaging system, both radiance from target and background falls in the detector. The information of solid-angle is given in Chapter 2. The solid-angle of imaging system as viewed from background and target is computed separately with using formulated in Equation 2.5. However, the assumption in this work is that R is the distance generally large and area might be specified with regard to infrared imaging diameter reformulated as given in Equation 4.6 and Equation 4.7

$$\Omega_{trgt} = \frac{\pi}{4}(\frac{D_{opt}}{R_{trgt}})^2. \tag{4.6}$$

$$\Omega_{bckgrnd} = \frac{\pi}{4}(\frac{D_{opt}}{R_{bckgrnd}})^2. \tag{4.7}$$

The total power collected at the detector when the target iexists is the aggregate of the power owing to the target and the background which is not concealed at the rear of the target. First step to determine the total power is that power coming from target and background must be calculated individually. The detector is collected the power per unit area coming from the target is given in Equation 4.8 and equivalently, the power per unit area from the background is specified by Equation 4.9

$$\frac{Power_{trgt}}{unitarea} = \Omega_{trgt}\tau_{opt}L_{trgt}\tau_{atm}. \tag{4.8}$$

$$\frac{Power_{bckgrnd}}{unitarea} = \Omega_{bckgrnd}\tau_{opt}L_{bckgrnd}\tau_{atm}. \tag{4.9}$$

Here, $Power_{trgt}$ is the power from target, $Power_{bckgrnd}$ is the power from background, τ_{atm} is the atmospheric transmittance, τ_{opt} is the transmittance of imaging system, L_{trgt} is the radiance of target, $L_{bckgrnd}$ is the radiance of background, Ω_{trgt} is the solid angle of infrared imaging system as viewed by the target, $\Omega_{bckgrnd}$ is the solid angle of infrared imaging system as viewed by the background.

Nevertheless, for the more calculations, such as the range prediction, the power unit area is multiplied by the specific target area to obtain the total power thanks to target as specified in Equation 4.10

$$Power_{trgt} = \Omega_{trgt}\tau_{opt}A_{trgt}L_{trgt}\tau_{atm}. \tag{4.10}$$

Similarly, the power unit area is multiplied by the specific background area to obtain total power owing to background as given in Equation 4.11

$$Power_{bckgrnd} = \Omega_{bckgrnd}\tau_{opt}A_{bckgrnd}L_{bckgrnd}\tau_{atm}. \tag{4.11}$$

When the target is present, the total power is calculated by Equation 4.12

$$Power_{total} = Power_{bckgrnd} + Power_{trgt}. \tag{4.12}$$

The other situation is that there is no target, background power is calculated with using image plane area as given in Equation 4.13

$$Power_{imgpln} = \Omega_{imgpln}\tau_{opt}A_{imgpln}L_{bckgrnd}\tau_{atm}. \tag{4.13}$$

For any target to be noticed, the difference of total power collected at the infrared imaging system when the target is existing and that of just background (image plane) ought to be a large amount than least distinguishable power of the infrared detector [17]. Distinguishable power of the infrared is defined as product of total noise, which is sum of the detector noise, i.e., noise equivalent power (NEP) and noise from temperature fluctuations in image plane [35], and signal-to-noise ratio (SNR) [34] as specified in Equation 4.14

$$Power_{total} - Power_{imgpln} \geq (SNR)(T.Noise). \tag{4.14}$$

To obtain range prediction, total power given in Equation 4.12 should be inserted in Equation 4.14. And then, the expression of power of target, background and image plane is given Equation 4.10, 4.11, 4.13, respectively should be inserted in Equation 4.15a

$$Power_{bckgrnd} + Power_{trgt} - Power_{imgpln} \geq (SNR)(T.Noise). \tag{4.15a}$$

$$\begin{aligned}(\Omega_{bckgrnd}\tau_{opt}A_{bckgrnd}L_{bckgrnd}\tau_{atm}) + (\Omega_{trgt}\tau_{opt}A_{trgt}L_{trgt}\tau_{atm}) - \\ (\Omega_{imgpln}\tau_{opt}A_{imgpln}L_{bckgrnd}\tau_{atm}) \geq (SNR)(T.Noise).\end{aligned} \tag{4.15b}$$

In addition to these steps, solid angle of infrared imaging system as viewed by target, background and image plane with using Equation 4.6 and area of background as given

in Equation 4.5 put in the Equation 4.15b

$$(\frac{\pi}{4}(\frac{D_{opt}}{R_{bckgrnd}})^2\tau_{opt}(A_{imgpln}-A_{trgt})L_{bckgrnd}\tau_{atm})+(\frac{\pi}{4}(\frac{D_{opt}}{R_{trgt}})^2\tau_{opt}A_{trgt}L_{trgt}\tau_{atm})- (\frac{\pi}{4}(\frac{D_{opt}}{R_{imgpln}})^2\tau_{opt}A_{imgpln}L_{bckgrnd}\tau_{atm}) \geq (SNR)(T.Noise). \tag{4.16}$$

The scenario for this thesis is that all distances ($R_{trgt} = R_{bckgrnd} = R_{imgpln} =$ R) from detector are equal. In order to simplify, Equation 4.16 can be rewritten owing to all common multiples or symbols.

$$(\frac{\pi}{4}(\frac{D_{opt}}{R})^2\tau_{opt}\tau_{atm})[((A_{imgpln}-A_{trgt})L_{bckgrnd})+(A_{trgt}L_{trgt})-(A_{imgpln}L_{bckgrnd})] \geq (SNR)(T.Noise). \tag{4.17a}$$

$$(\frac{\pi}{4}(\frac{D_{opt}}{R})^2\tau_{opt}\tau_{atm})[((A_{imgpln}L_{bckgrnd}-A_{trgt}L_{bckgrnd})+(A_{trgt}L_{trgt})- (A_{imgpln}L_{bckgrnd})] \geq (SNR)(T.Noise). \tag{4.17b}$$

$$(\frac{\pi}{4}(\frac{D_{opt}}{R})^2\tau_{opt}\tau_{atm})[A_{trgt}(L_{trgt}-L_{bckgrnd})] \geq (SNR)(T.Noise). \tag{4.17c}$$

If the R is revised, the theoretically range prediction formula of the imaging system is derived an given in Equation 4.18

$$R \leq \sqrt{\frac{\pi(D_{opt})^2\tau_{opt}\tau_{atm}A_{trgt}(L_{trgt}-L_{bckgrnd})}{4(SNR)(T.Noise)}}. \tag{4.18}$$

The maximum value of range prediction is the one situation that left and right sides of the Equation 4.18 are equal to each other.

4.7 Range Discrimination Methodology in IR Signature Model

In this thesis study, Johnson Criterion which is the simplest method for the range discrimination methodology is utilized. According to the Johnson criterion, it is assumed that the target is at the center of the field of view of imaging system and that the imaging system does not need to find the target [27]. Within the Johnson criterion, three various discrimination term are defined for the range: Detection, Recognition and Identification. That criterion also defines the minimum number of cycles required for the calculation of range. The minimum number of cycles required for range prediction value with the probability of 50% is defined as one for the detection, four for the recognition and eight for the identification [27]. However, if the lower and/or higher probability is demanded, Johnson criterion provides some multipliers and that is stated in Table 4.1.

Table 4.1: Value of probability and multiplier [27].

Probability(%)	**Multiplier**
100	3.0
95	2.0
80	1.5
50	1.0
30	0.75
10	0.50
2	0.25
0	0

For the target with massive aspect ratio, a number of pixels are used in preference to that of cycles as claimed by Johnson Criteria. Although the number of pixels and cycles are not the same and these are not replaced by each other, the use of Nyquist Criteria is appropriate when the pixels are at issue. In keeping with Nyquist Criteria, two pixels are required for one cycle [27]. The total number of pixels for two pixels per cycle is given Equation 4.19

$$N_{pixels} = (2N_{\mathrm{x}})(2N_y) \tag{4.19}$$

Here, N_x is horizontal number of cycles, N_y is vertical number of cycles, N_{pixels} is the total number of pixel in the detector.

Next chapter is that calculation and results of the radiometry-based range prediction for both band and effects of particular parameters on range performance is investigated.

CHAPTER 5

COMPUTATIONAL RANGE PREDICTION

This chapter computes range predictions at MWIR and LWIR spectral band for particular target, background, optics, detectors, and SNR parameters using the theoretical formula driven in Chapter 4, and the results of atmospheric transmittance of MWIR and LWIR spectral bands calculated with using MODTRAN^{TM}5 in Chapter 3. Furthermore, the impact of the change in some of those parameters on the prediction results are presented in this chapter.

5.1 Particular Parameters

The technical specifications and values of parameters for both spectral bands are chosen, and they are given in Table 5.1 $-$ 5.6, respectively.

Table 5.1: The technical specifications and values of detector

Technical Specifications	**MWIR**	**LWIR**
Infrared Spectral Band (μm)	3.6 - 4.9	7.7 - 9.3
Focal Plane Array (FPA)	640 X 512	640 X 512
Pixel Pitch (μm)	15	15
Noise-Equivalent Temperature Difference (NETD), (mK)	20	25
Noise-Equivalent Power (NEP), (W)	2.90 X 10^{-14}	2.70 X 10^{-13}
Noise-Equivalent Irradiance (NEI), (W\cm^2)	1.28 X 10^{-8}	1.26 X 10^{-7}

Table 5.2: The technical specifications and values of imaging system

Technical Specifications	**MWIR**	**LWIR**
Infrared Spectral Band (μm)	3.6 - 4.9	7.7 - 9.3
Focal Length (mm)	50	50
Aperture (mm)	25	25
F-Number	2	2
Field of View (FOV), (°)	14	14
Transmittance	0.81	0.81

Table 5.3: The technical specifications and values of target and background

Technical Specifications	**MWIR and LWIR**
Temperature of Target (K)	293.15 - 313.15
Emissivity of Target [32, 33]	0.54
Temperature of Background (K)	293.15
Emissivity of Background for Land, Sea and Air [32, 33]	0.90, 0.20 and 0.05

Table 5.4: The technical specifications and values of target size

Technical Specifications	**Width (m)**	**Length (m)**	**Height (m)**
Land : S-300 Launcher	2.75	11.3	2.85
Sea : Arleigh Bruker Destroyer	20.0	154.0	9.3
Air : F-16C	10.0	15.03	5.09

Table 5.5: The technical specifications and values of number of pixels

Technical Specifications	**Number of Pixel**
Detection	6
Recognition	24
Identification	48

Table 5.6: The technical specifications and values of atmospheric transmittance

Technical Specifications	**MWIR**	**LWIR**
Transmittance of Atmospheric Condition 1	0.47	0.26
Transmittance of Atmospheric Condition 2	0.44	0.25
Transmittance of Atmospheric Condition 3	0.31	0.20
Transmittance of Atmospheric Condition 4	0.10	0.08

5.2 Range Prediction for Mid- and Long-Wave Infrared Imaging System

This section investigates the detection, recognition and identification (DRI) ranges for land, sea and air targets using the aforementioned parameters, theirs values and the range prediction formula obtained in the Chapter 4. First, the noise and SNR terms in Equation 4.14 are determined. For this study, the SNR is chosen to be 3 dB. The noise distorts the real signal emitted from the target. This study assumes the noise constitutes the detector noise and background noise due to background temperature fluctuations, which is calculated. The detector noise, which is labeled as the Noise Equivalent Irradiance (NEI) or Noise Equivalent Power (NEP), is obtained for the detector data sheet. The advances in the technology enabled production of detectors with very low NEI and NEP. The background noise also is calculated using the Planck formula. As shown in Table 5.3, the background temperature is chosen to be 293.15 K . The background temperature distribution is not uniform. The temperature fluctuations in the background is modeled using MATLAB^{TM} random number generator with $\pm 2/3$ standard variation for 10000 different temperature points. For all temperatures values, the background radiances were calculated using the Planck equation. The mean value of the background radiances represents the background thermal noise. The sum of the background thermal noise and the detector noise represents the noise term in Equation 4.14.

The detection, recognition and identification (DRI) range predictions at a given atmospheric condition are calculated for both infrared imaging system using MATLAB^{TM}. The effect of the temperature difference between the target and background on the range predictions are shown in Figures $5.1 - 5.3$ for the mid-wave and Figures $5.4 - 5.6$ for long-wave, respectively.

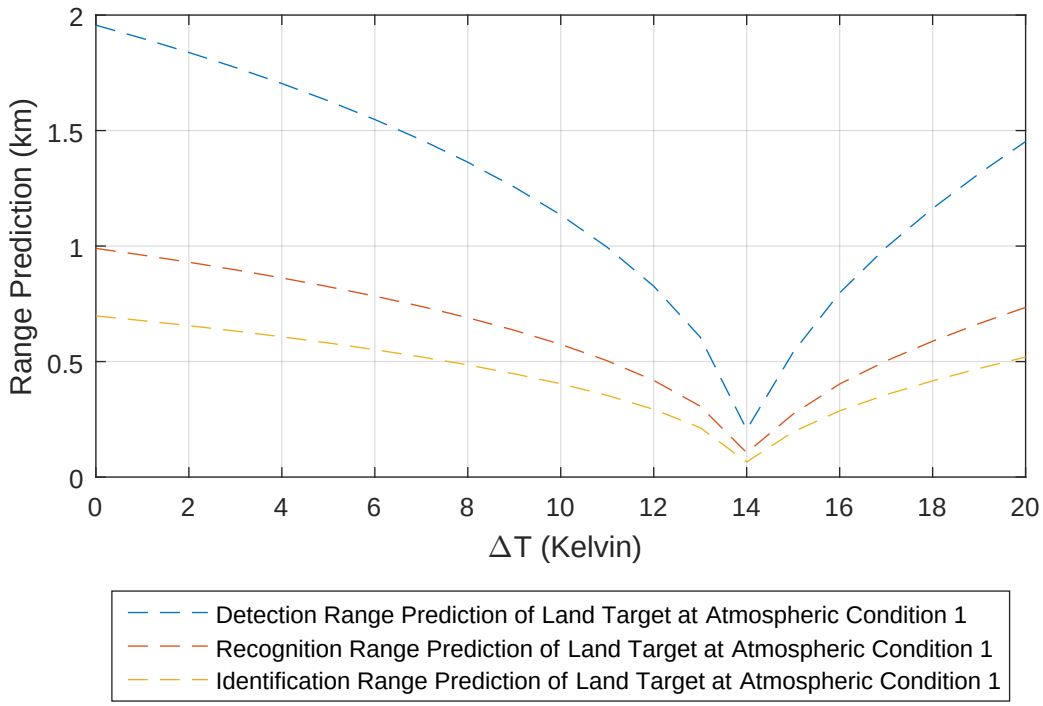

Figure 5.1: DRI ranges at MWIR of land target as function of AC 1

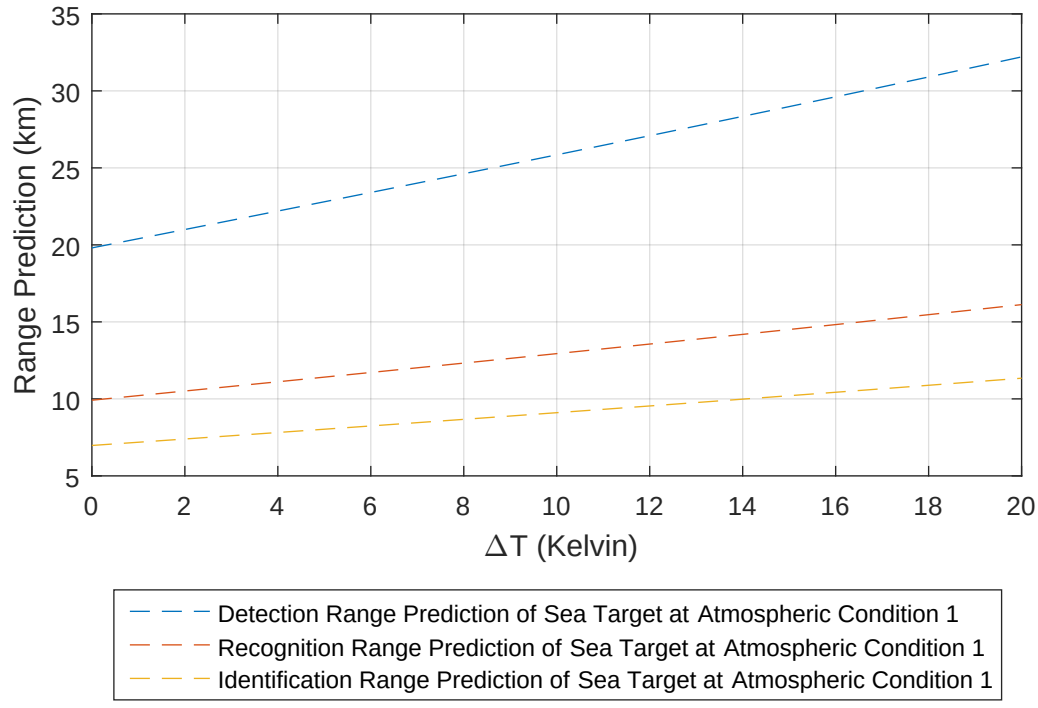

Figure 5.2: DRI ranges at MWIR of sea target as function of AC 1

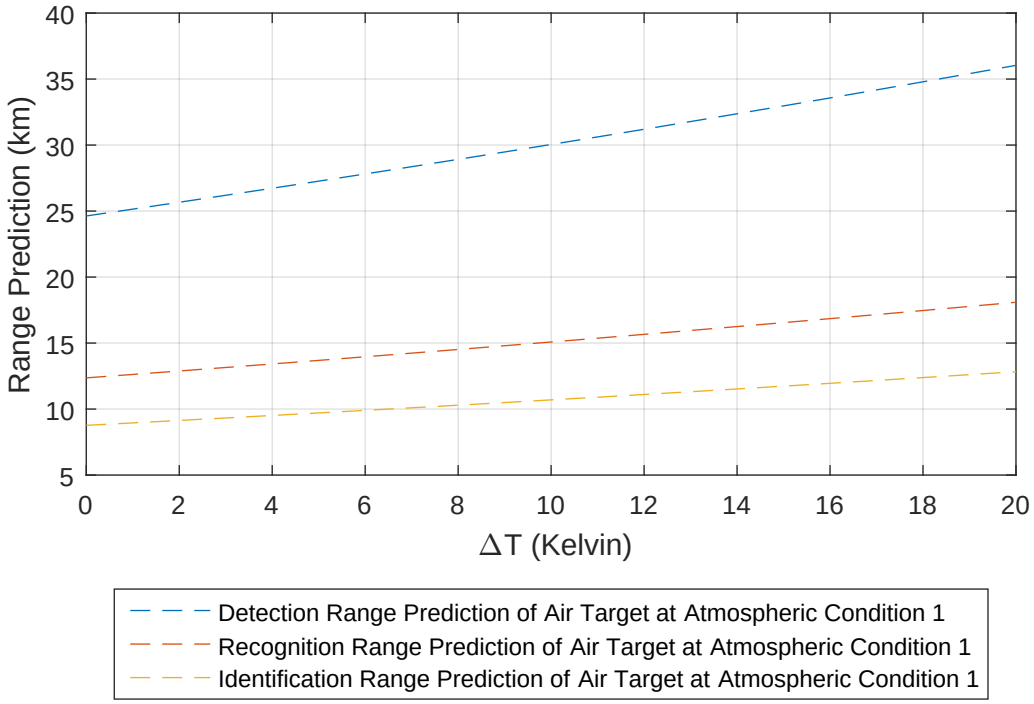

Figure 5.3: DRI ranges at MWIR of air target as function of AC 1

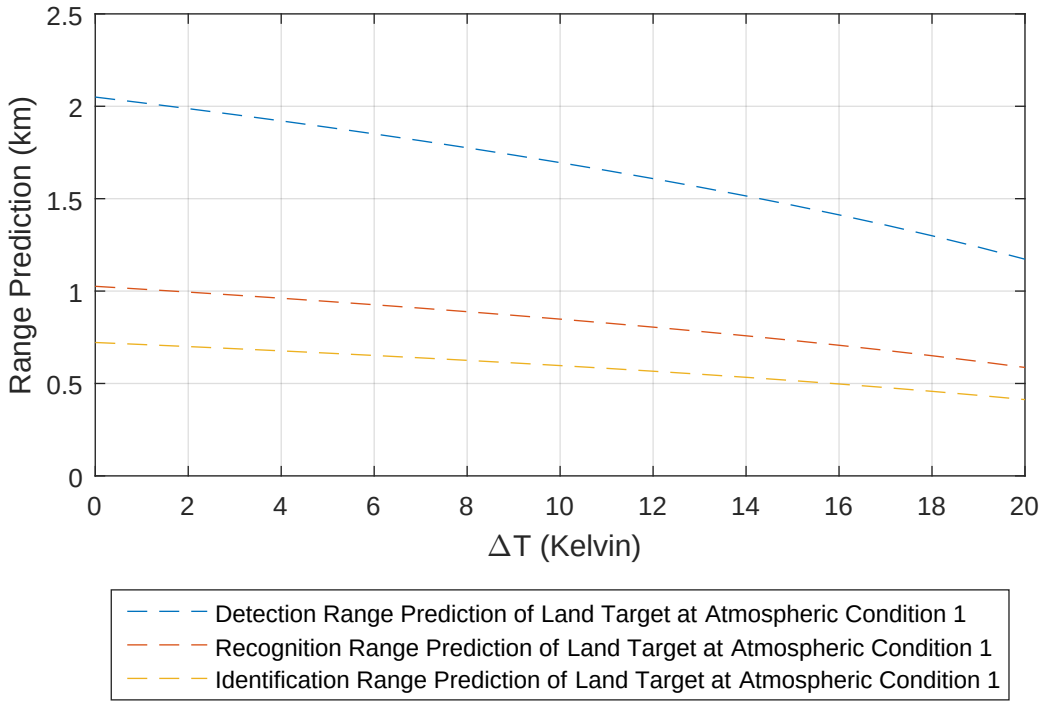

Figure 5.4: DRI ranges at LWIR of land target as function of AC 1

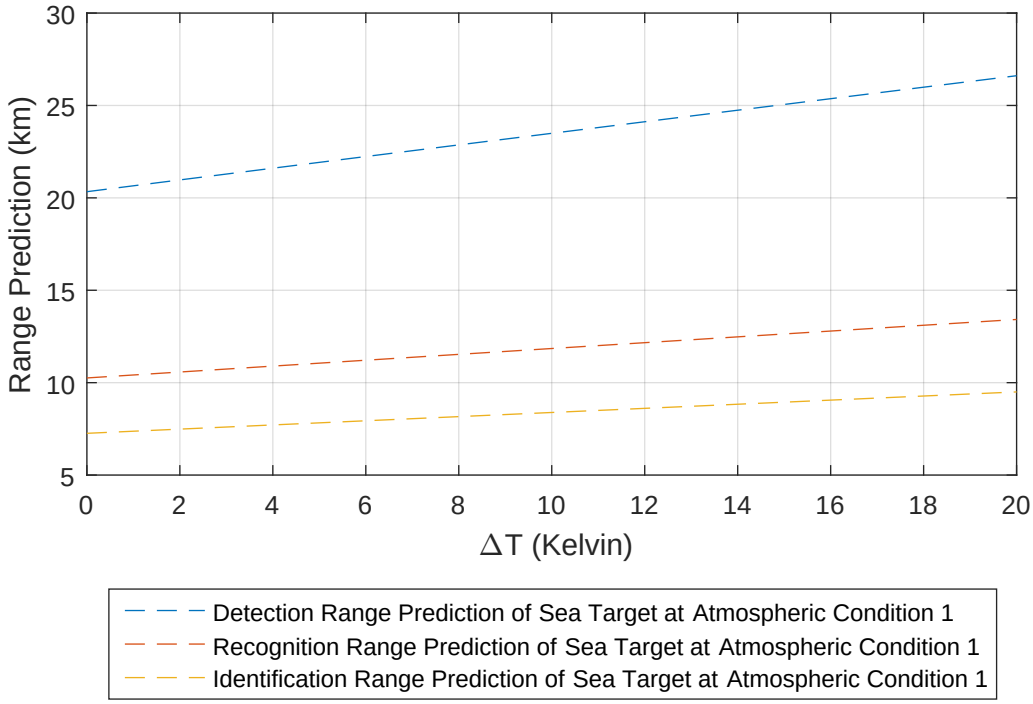

Figure 5.5: DRI ranges at LWIR of sea target as function of AC 1

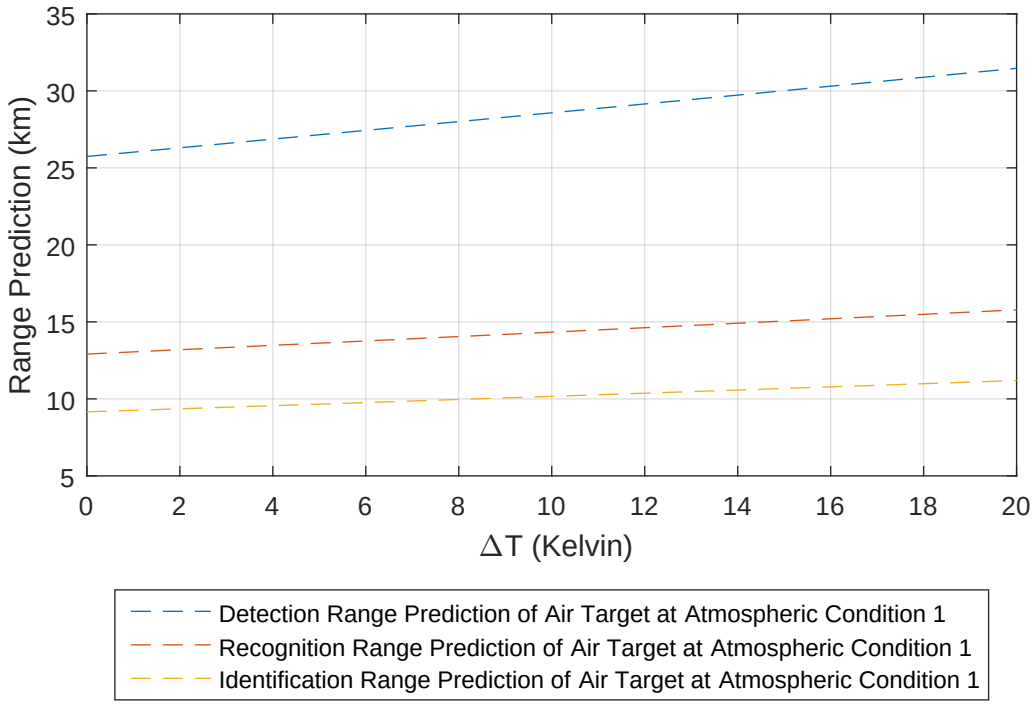

Figure 5.6: DRI ranges at LWIR of air target as function of AC 1

A range of 20 K, from 0 to 20 K with steps of 1 K, is used as temperature difference between the target and background (ΔT). The most interesting characteristics of the range predictions at mid-wave infrared imaging systems for three different target types is that DRI range predictions are decreasing for the land target, as the ΔT approaches 14 K. That characteristics is same for the long wavelengths, but the temperature difference increases from 14 to 20 K in long- wave infrared imaging systems. This result shows that up 14 and 20 K ΔT for the mid- and long-wave, respectively the background is more dominant than the target. This phenomenon is caused due to the emissivity coefficient. In this thesis, background is chosen to be soil and the emissivity coefficient of the soil is significantly higher than the coefficient of the steel, as given in Table 5.3. Calculations with these coefficients and the Planck equation show that the background radiates more than the target up to temperature difference of 14 and 20 K for the mid- and long-wave infrared imaging systems, respectively. For sea and air targets, range predictions do not show similar characteristics for the both bands, as the background emissivity coefficients for water and air are significantly lower than the steel. Table 5.3 shows coefficients for water and air as well. Finally, all figures for both bands show that DRI range prediction is possible at a ΔT of 0 K. The no temperature difference range predictions are possible because the difference in radiant coefficients causes different radiance between the target and the background even when there is no temperature difference between them.

5.2.1 The Effect of the Atmospheric Conditions on the Range

Keeping other variables constant, the effect of atmospheric transmittance on the range is investigated for land, sea, and air targets. Figures $5.7 - 5.9$ show DRI range predictions at MWIR for a land target for remaining three different atmospheric conditions, given in Table 3.2.

Figures $5.10 - 5.12$ show DRI range predictions at LWIR for a land target for remaining three different atmospheric conditions, given in Table 3.2.

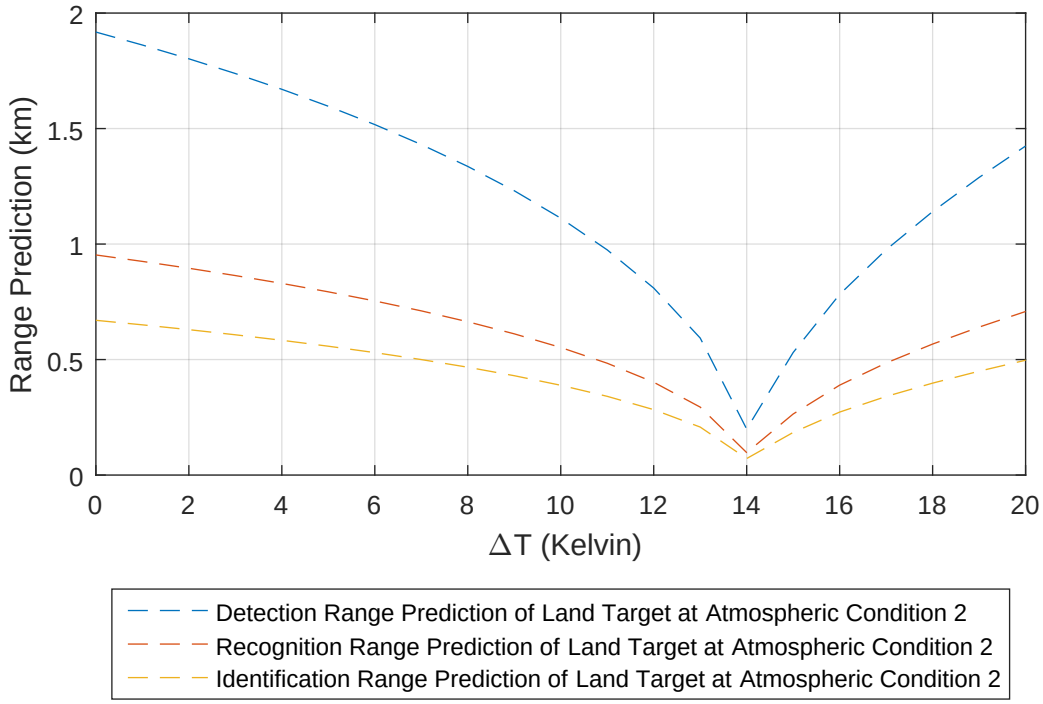

Figure 5.7: DRI ranges at MWIR of land target as function of AC 2

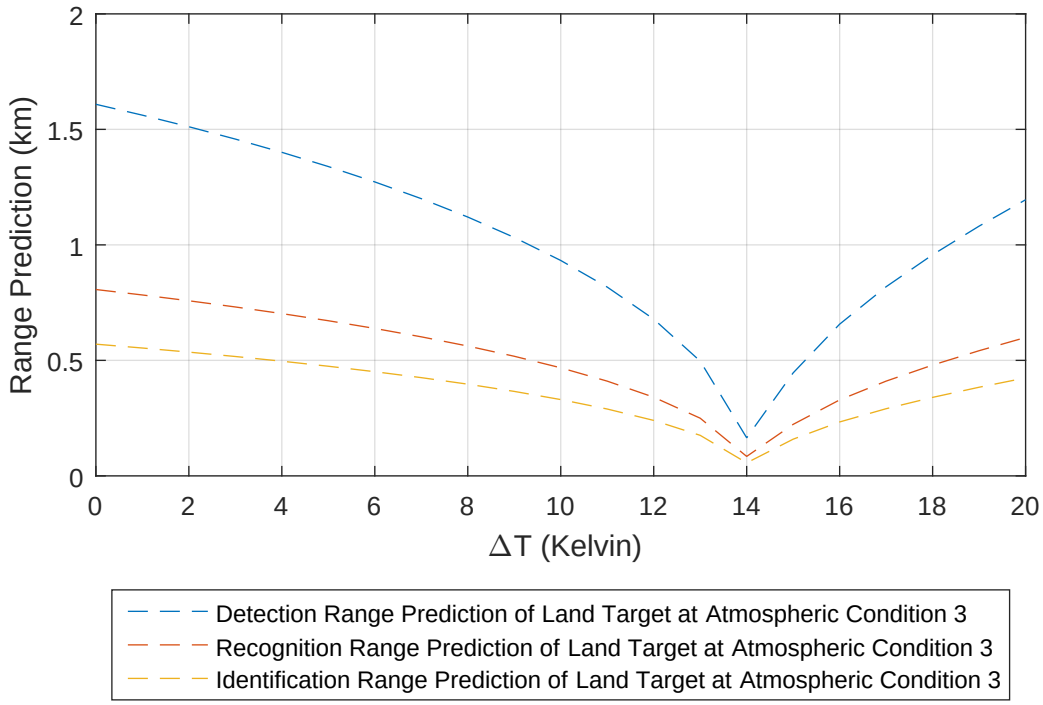

Figure 5.8: DRI ranges at MWIR of land target as function of AC 3

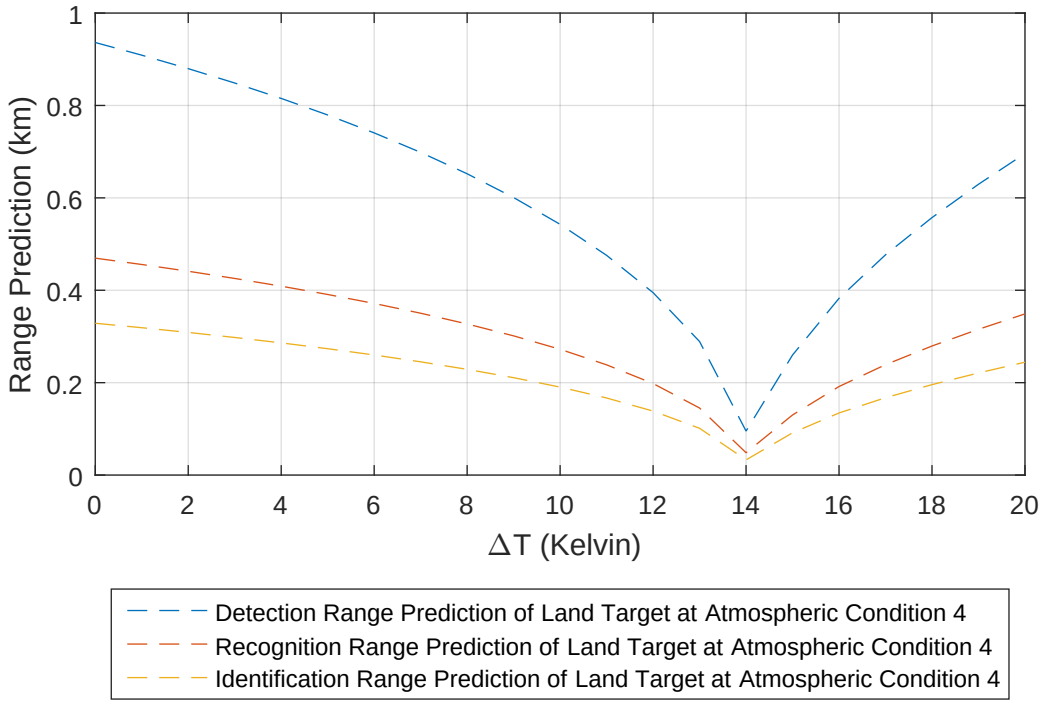

Figure 5.9: DRI ranges at MWIR of land target as function of AC 4

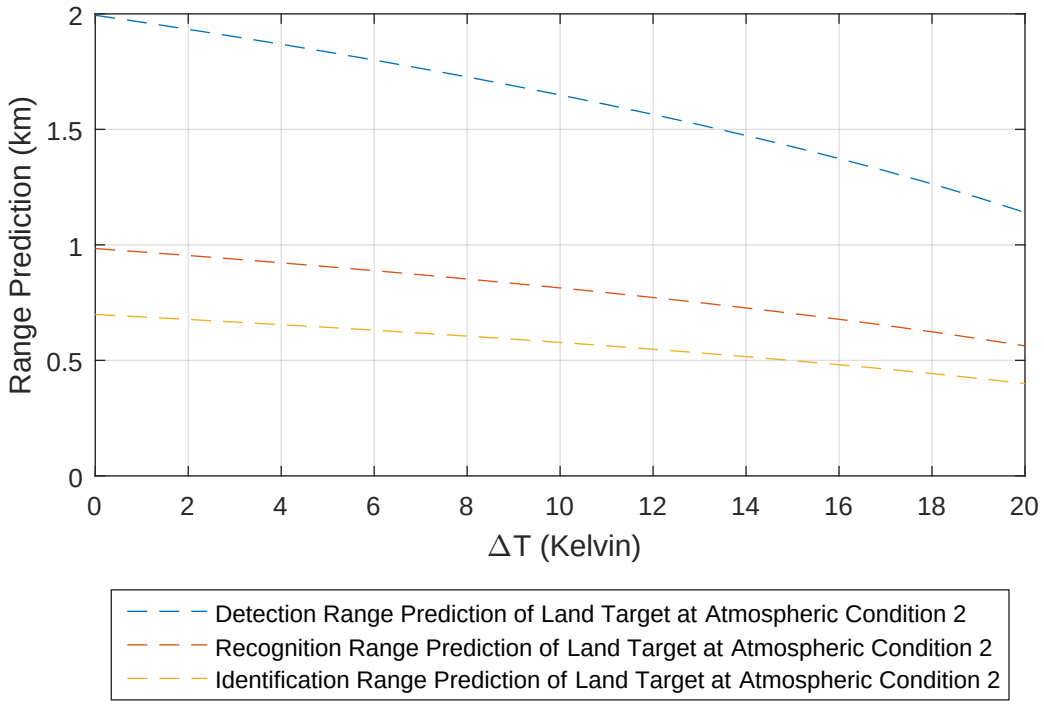

Figure 5.10: DRI ranges at LWIR of land target as function of AC 2

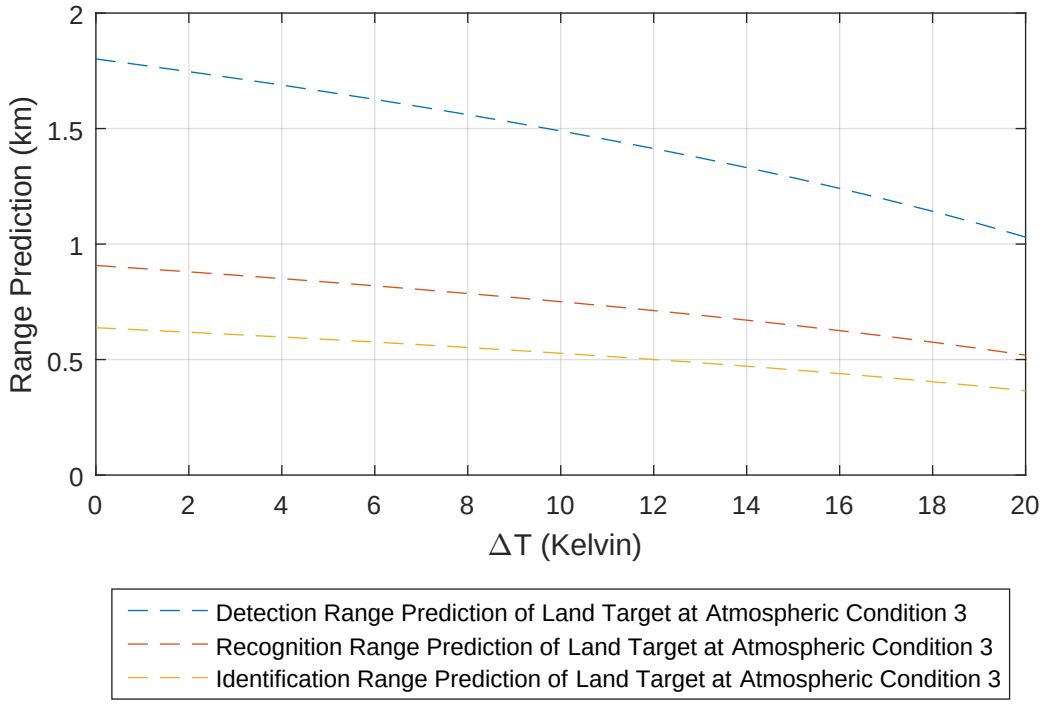

Figure 5.11: DRI ranges at LWIR of land target as function of AC 3

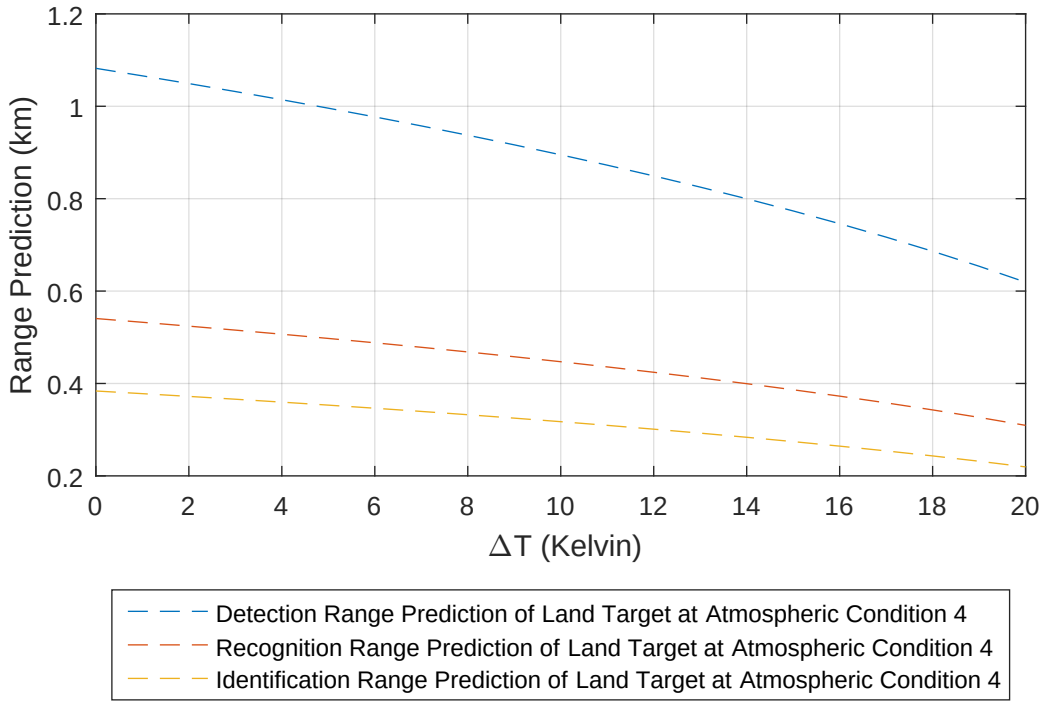

Figure 5.12: DRI ranges at LWIR of land target as function of AC 4

The land target range predictions same characteristics similar to the previous study, shown in Figure 5.1. This results demonstrates that changes in atmospheric conditions only affect the value of the range prediction. Atmosphere changes do not affect the characteristics of the range prediction curves.

Same study is repeated for a sea target for three different atmospheric conditions and the results are shown in Figures 5.13 − 5.15 for MWIR and Figures 5.16 − 5.18 for LWIR .

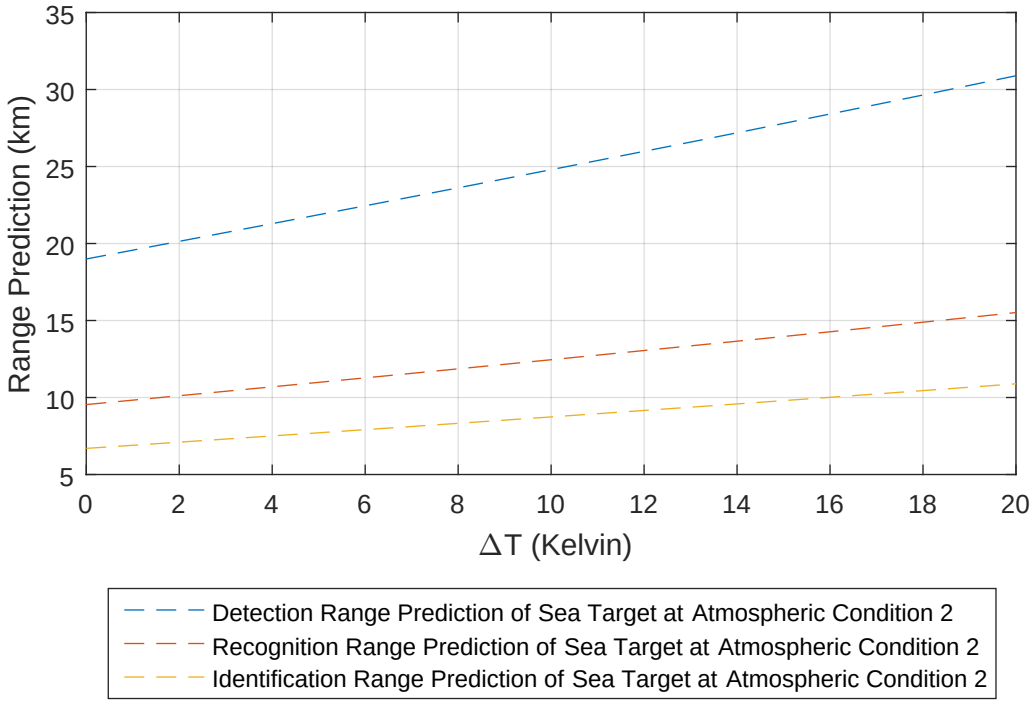

Figure 5.13: DRI ranges at MWIR of sea target as function of AC 2

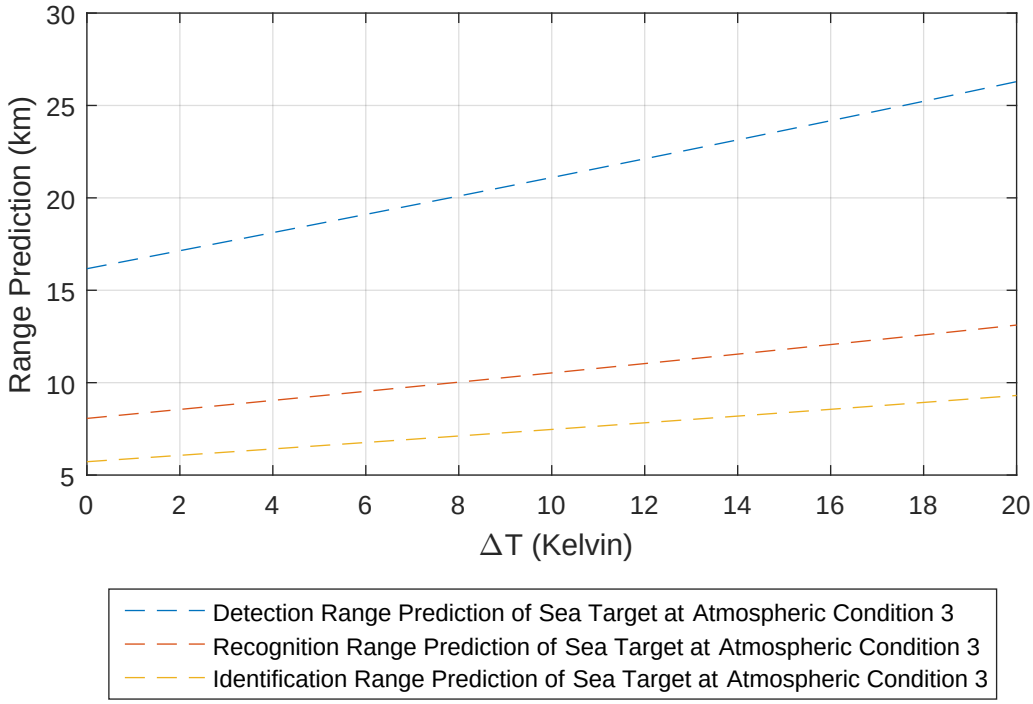

Figure 5.14: DRI ranges at MWIR of sea target as function of AC 3

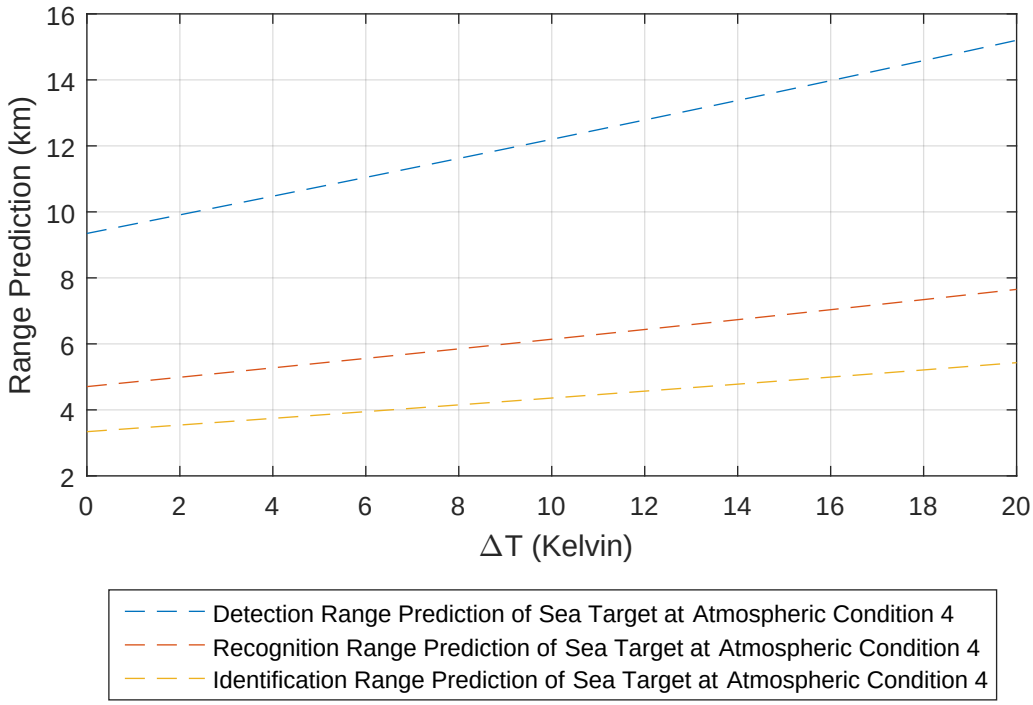

Figure 5.15: DRI ranges at MWIR of sea target as function of AC 4

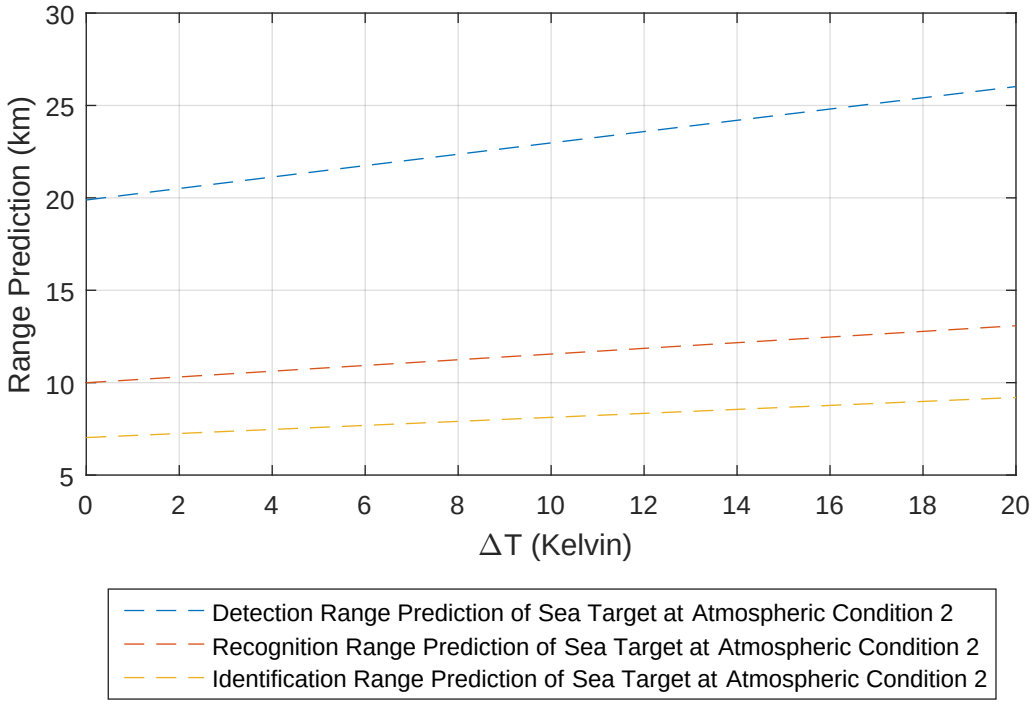

Figure 5.16: DRI ranges at LWIR of sea target as function of AC 2

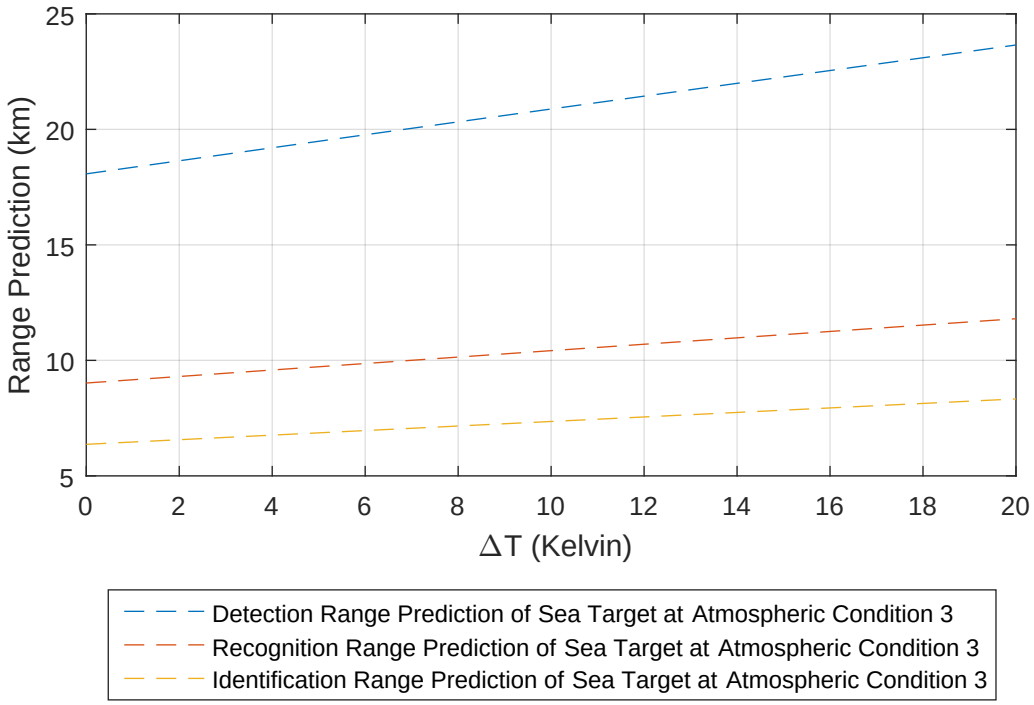

Figure 5.17: DRI ranges at LWIR of sea target as function of AC 3

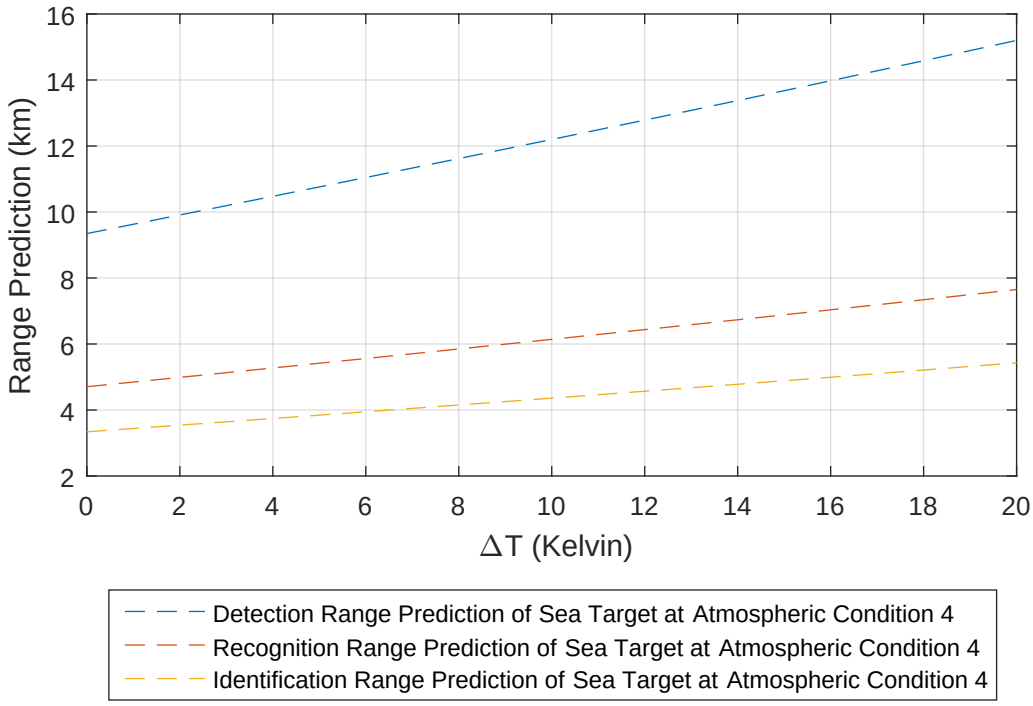

Figure 5.18: DRI ranges at LWIR of sea target as function of AC 4

Similarly, results for an air target are presented in Figures 5.19 – 5.21 for MWIR and Figures 5.22 – 5.24 for LWIR, respectively.

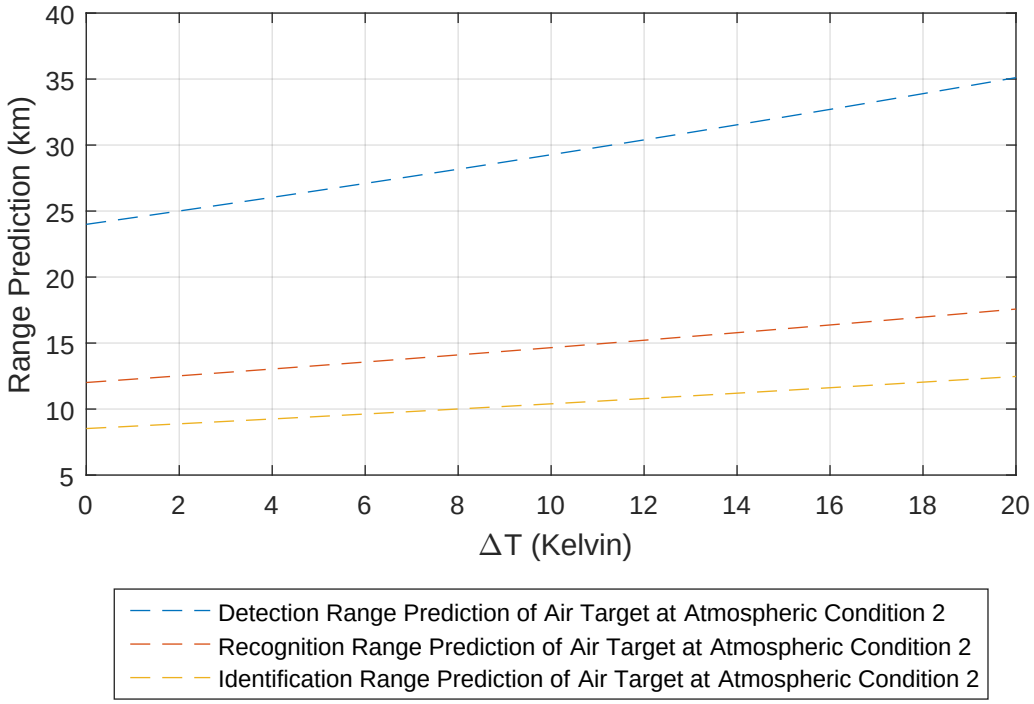

Figure 5.19: DRI ranges at MWIR of air target as function of AC 2

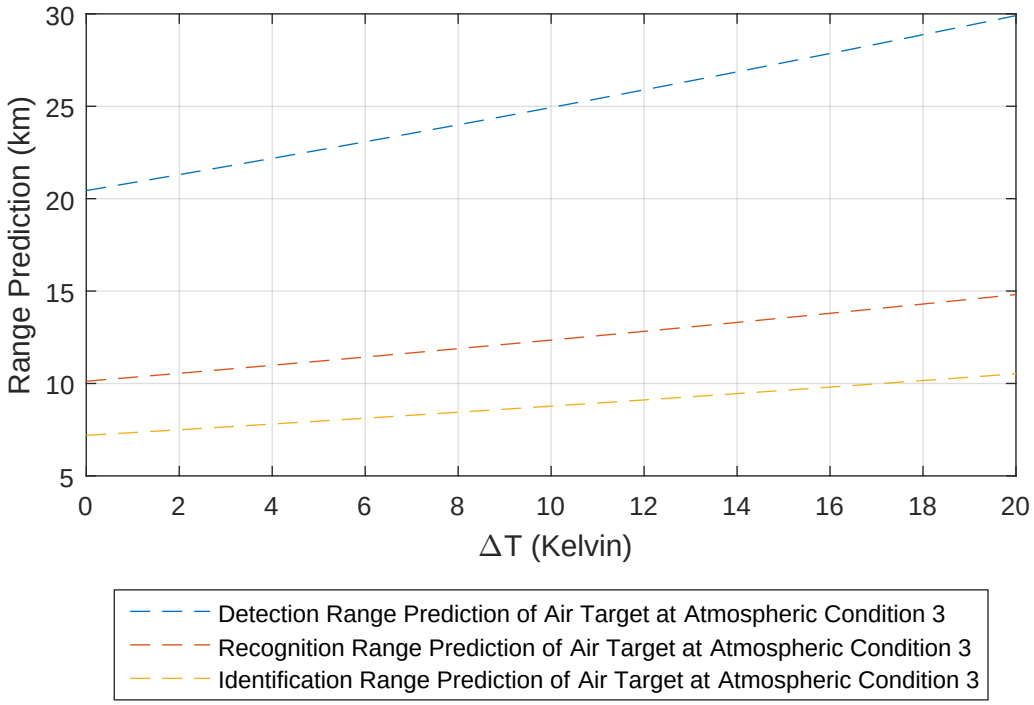

Figure 5.20: DRI ranges at MWIR of air target as function of AC 3

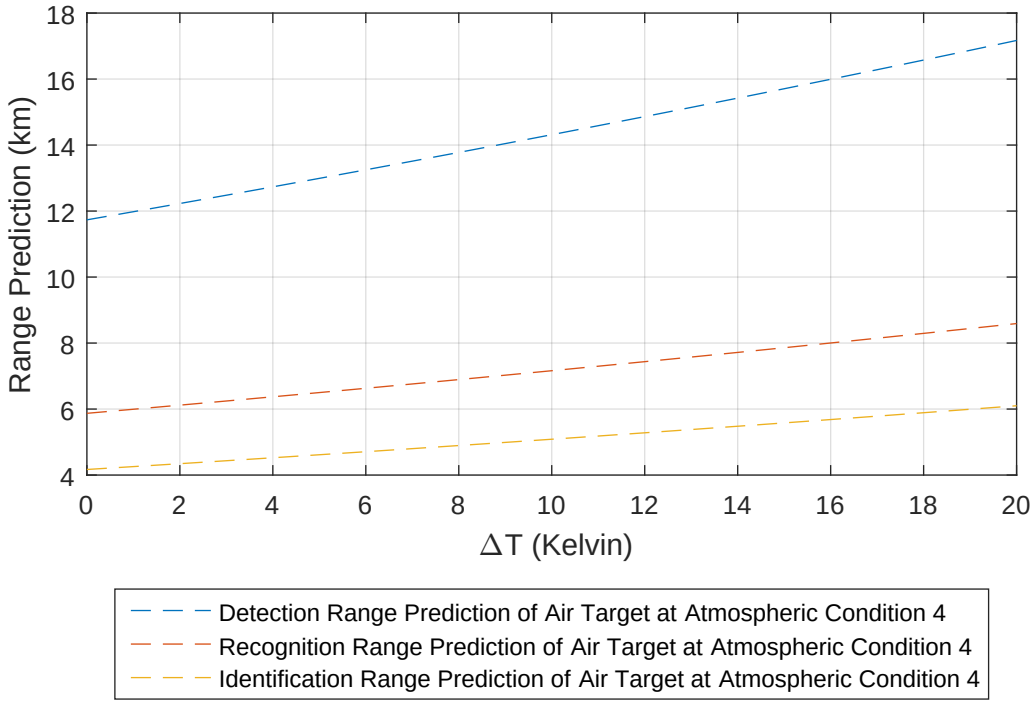

Figure 5.21: DRI ranges at MWIR of air target as function of AC 4

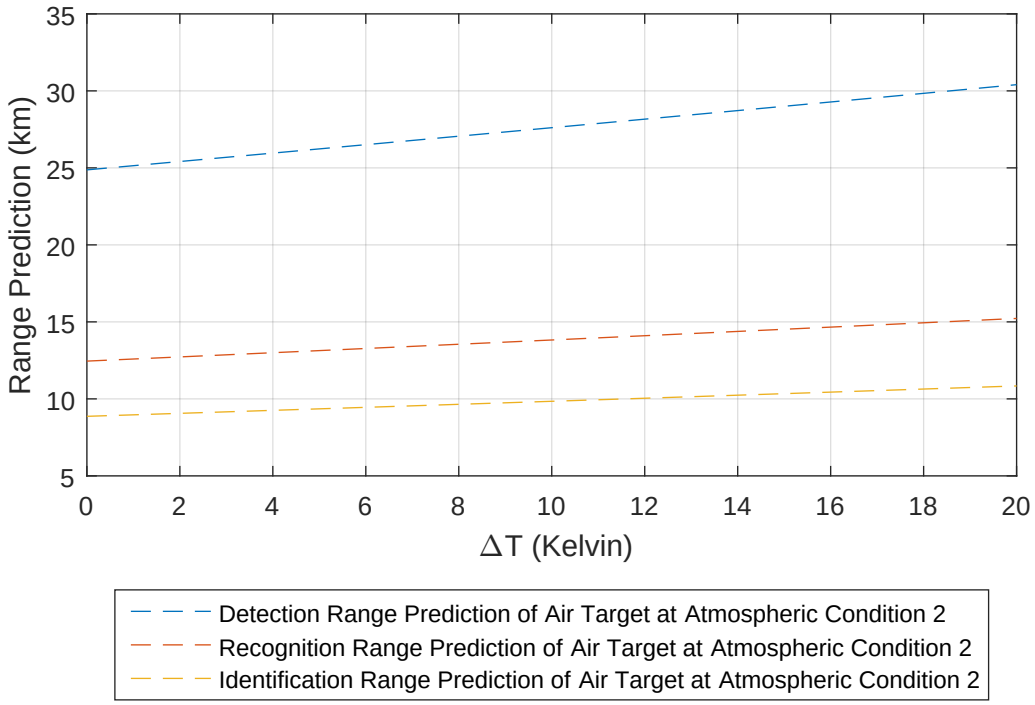

Figure 5.22: DRI ranges at LWIR of air target as function of AC 2

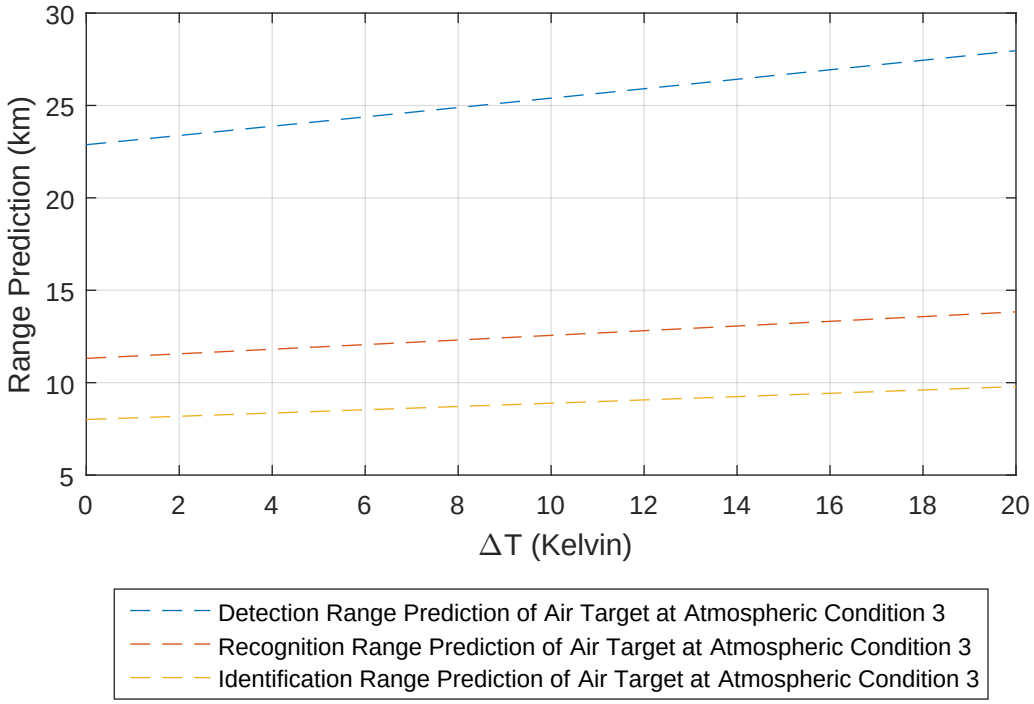

Figure 5.23: DRI ranges at LWIR of air target as function of AC 3

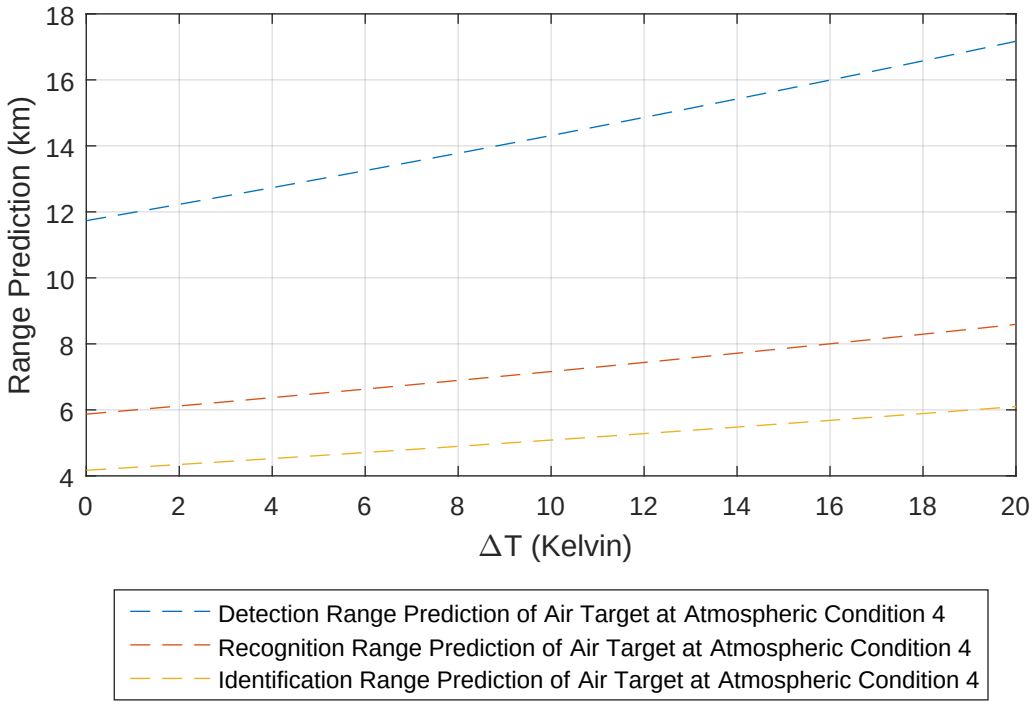

Figure 5.24: DRI ranges at LWIR of air target as function of AC 4

All the results show that the range prediction values are highest for the first atmospheric condition for all types of targets at all temperature difference values. For the land target, results show that the DRI range values at MWIR for the first atmospheric condition are 3.11, 18.16, and 52.53% higher from results obtained at the second, third, and the fourth atmospheric conditions respectively. Similar trends observed for sea and air target types study. The range predictions at the first atmospheric condition are higher by 3.93, 18.31, and 52.48%. The air target values are 2.73, 17.70, and 59.50%. Furthermore, the DRI range values at LWIR for the first atmospheric condition are 3.33, 11.77, and 47.10% higher from results obtained at the second, third, and the fourth atmospheric conditions respectively. The sea target values are 2.62, 11.81, and 46.69%. The air target values are 3.63, 12.02, and 47.00%.

This study and results suggest that the rain is the most important atmospheric factor. Raindrops absorb the radiation significantly causing performance degrade. Another important factor is the visibility. When visibility range drops down from 23 to 5 km, which represents the switch between atmospheric condition two to three, the detection range drops by 16.16%, the recognition range drops by 15.24%, and the identification range drops by 15.14% for the land target at MWIR. These values are 9.66, 7.77, and 8.71% for the LWIR band. These values at MWIR are 14.89, 15.46, and 14.53% for sea target; 14.81, 15.72, and 15.61% for the air target. For the LWIR, the detection range drops by 9.10%, the recognition range drops by 9.76%, and the identification range drops by 9.44% for the sea target; 8.01, 9.14, and 9.70% for the air target.

In conclusion, as expected, results demonstrate that the decrease in atmospheric transmittance values for both bands decreases the range prediction.

5.2.2 The Effect of the Optical Aperture on Range

This section studies the impact of the optical aperture of the infrared imaging system on the range predictions. The aperture size is changed between 10 and 50 mm with 5 mm steps. Figures 5.25 – 5.27 show DRI range predictions at MWIR as a function of ΔT at different aperture sizes.

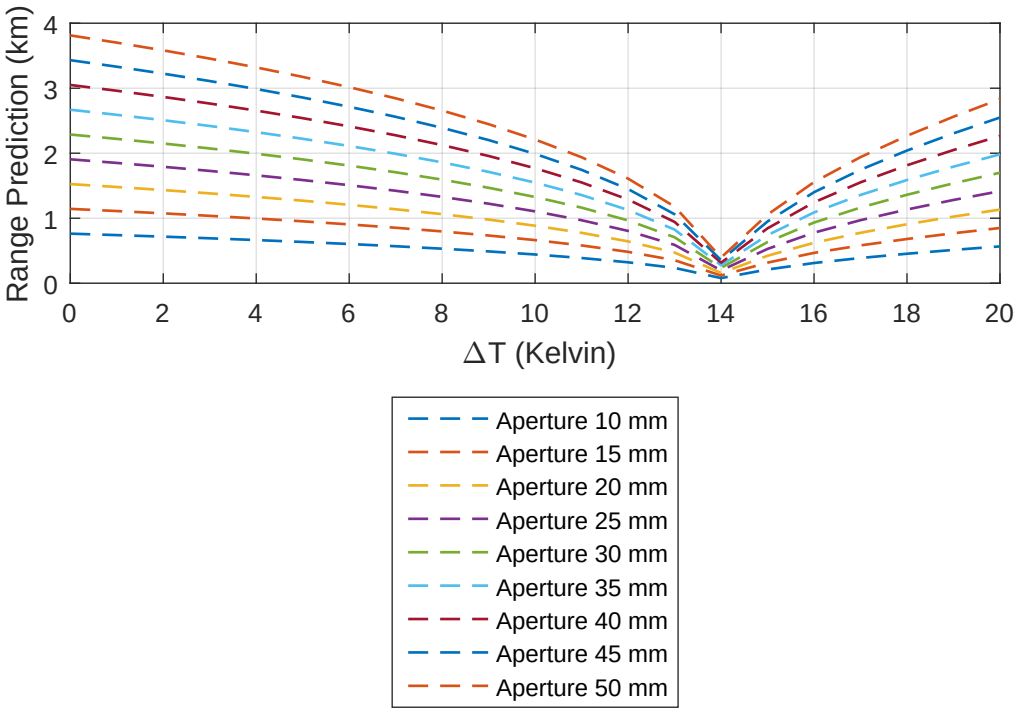

Figure 5.25: Detection range of land target at MWIR as function of aperture at AC 2

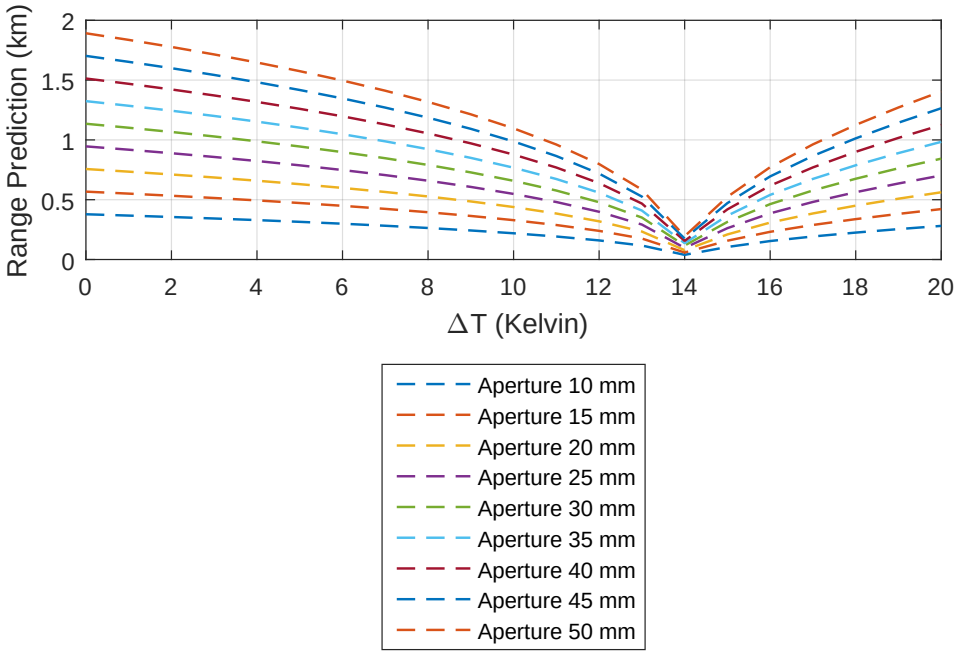

Figure 5.26: Recognition range of land target at MWIR as function of aperture at AC 2

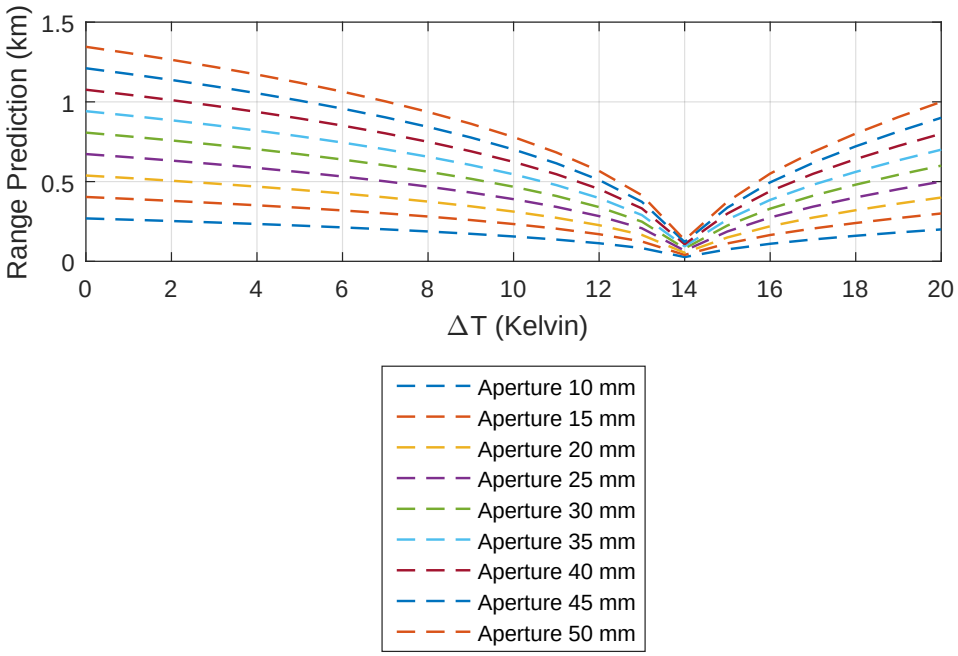

Figure 5.27: Identification range of land target at MWIR as function of aperture at AC 2

Similar trends are also observed in this atmospheric condition for LWIR as well. The effect of the change in aperture size on the range predictions at LWIR for a land target is depicted in Figures 5.28 – 5.30.

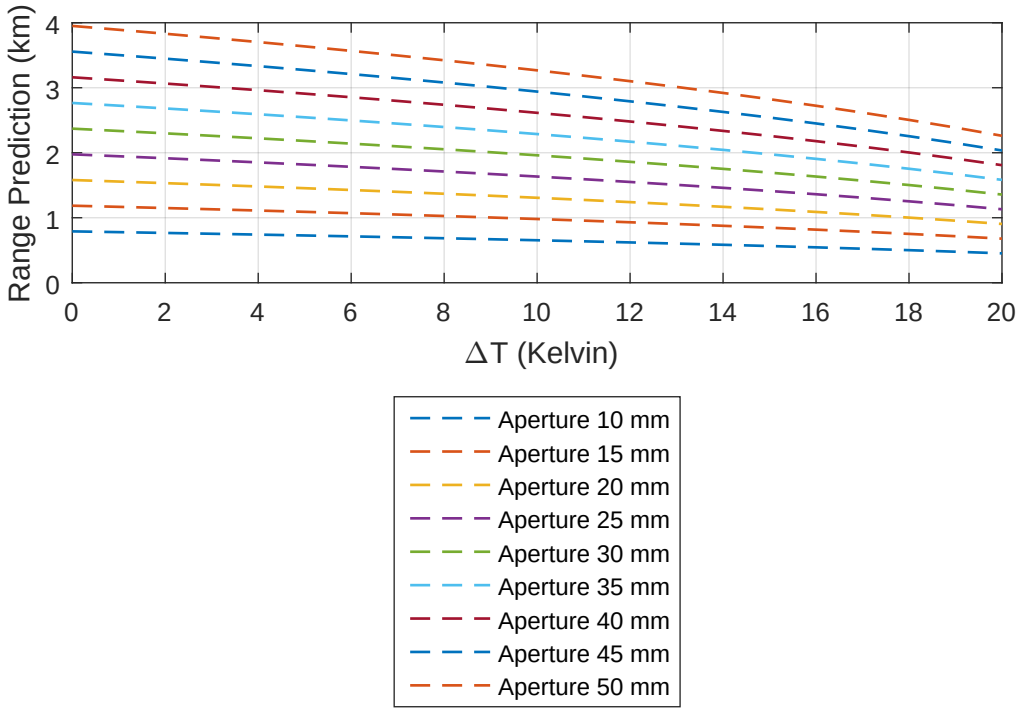

Figure 5.28: Detection range of land target at LWIR as function of aperture at AC 2

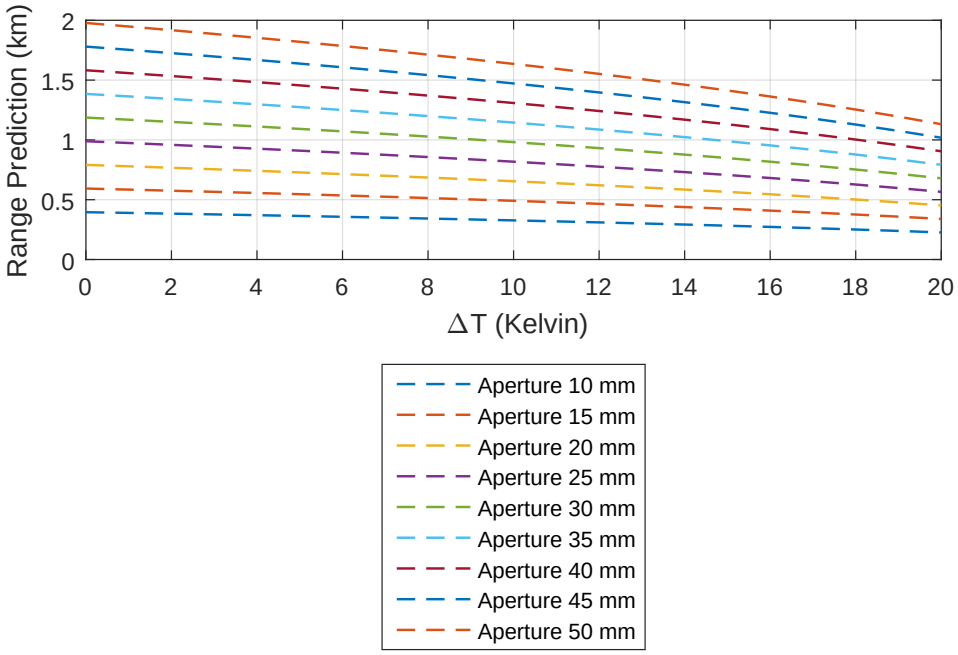

Figure 5.29: Recognition range of land target at LWIR as function of aperture at AC 2

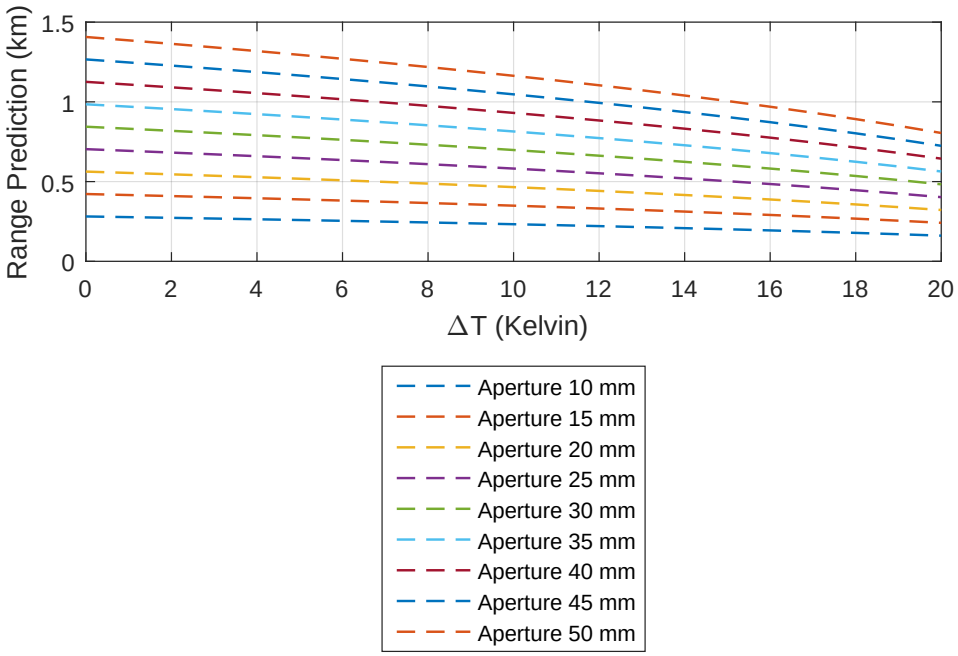

Figure 5.30: Identification range of land target at LWIR as function of aperture at AC 2

At the second atmospheric conditions and keeping other variables constant, for the land target, results show that the DRI range predictions increase as the aperture size increases. The reason is that the imaging system with larger aperture size naturally collects more radiance. When the aperture is changed from 10 to 50 mm, the increase in DRI range prediction is 400% at both band for the land target. For example, the detection range at MWIR at 0 K ΔT for 10 mm aperture size is 0.76 km, whereas it is 3.83 km for an aperture size of 50 mm. For the LWIR, these values are 0.78 km and 3.94 km, respectively.

For the other remaining atmospheric conditions and target types at both bands, when the aperture size is changed from 10 to 50 mm, DRI ranges prediction is raised by 400%.

5.2.3 The Effect of the Optical Transmittance on Range

This section investigates the impact of the optical transmittance of the mid- and long-wave infrared imaging system on the range predictions. The optical transmittance is altered between 0 and 1.00 with 0.25 steps. For both band, if the optical transmittance value is the zero, result of range prediction can not be estimated because radiance from target can not fall in the detector through the optical system. In addition, a value of 1.00 for the transmittance represents the ideal situation.

Figures 5.31 $-$ 5.33 show DRI range predictions at MWIR as a function of ΔT at various optical transmittance.

Similar trends are also observed in this atmospheric condition for LWIR as well. The effect of the change in optical transmittance on the range predictions at LWIR for a land target is depicted in Figures 5.34 $-$ 5.36.

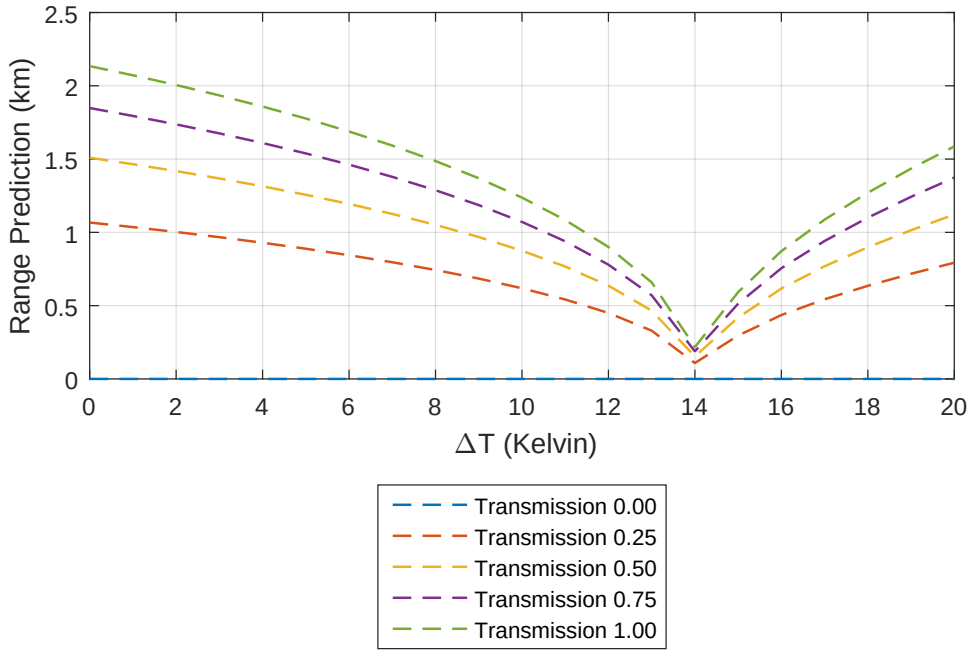

Figure 5.31: Detection range of land target at MWIR as function of optical transmittance at AC 2

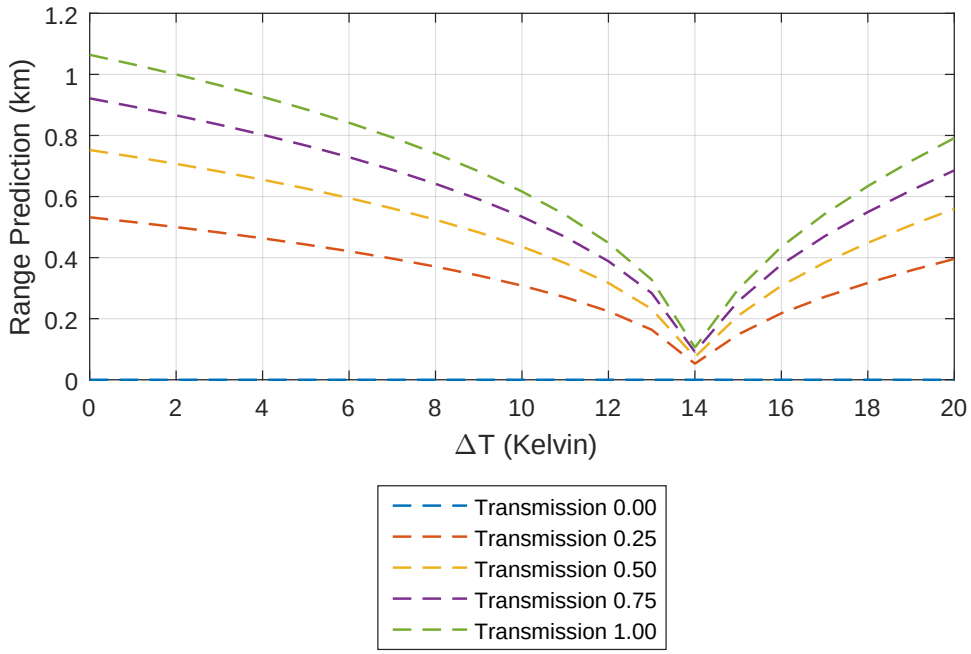

Figure 5.32: Recognition range of land target at MWIR as function of optical transmittance at AC 2

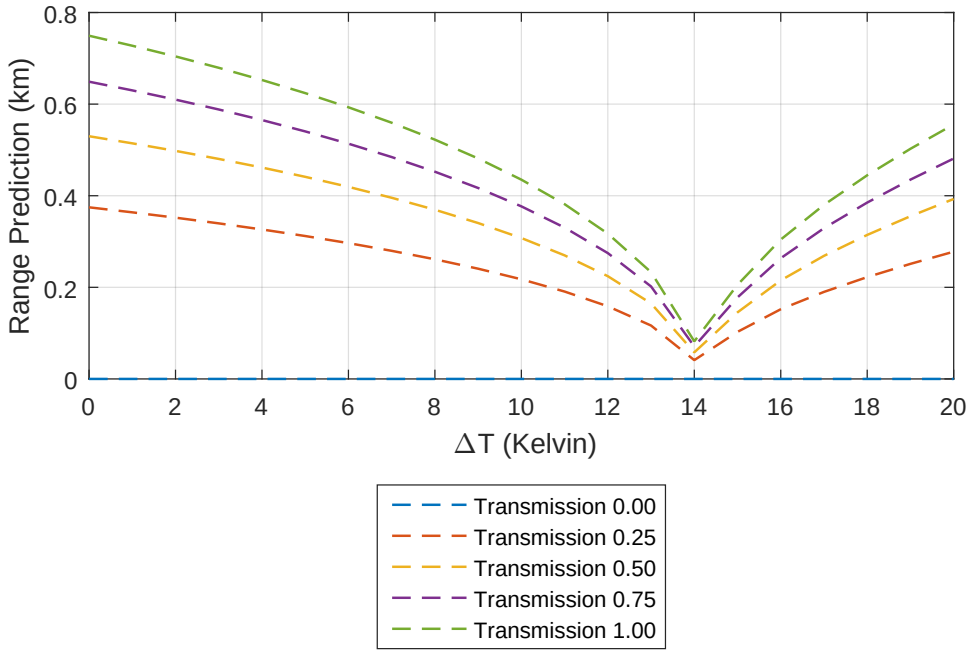

Figure 5.33: Identification range of land target at MWIR as function of optical tansmittance at AC 2

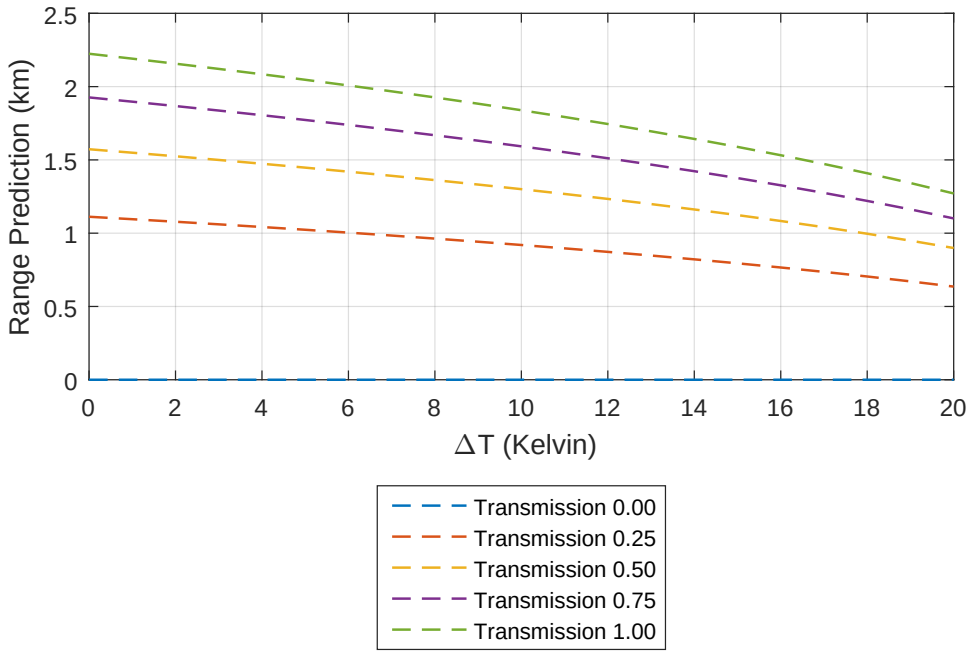

Figure 5.34: Detection range of land target at LWIR as function of optical transmittance at AC 2

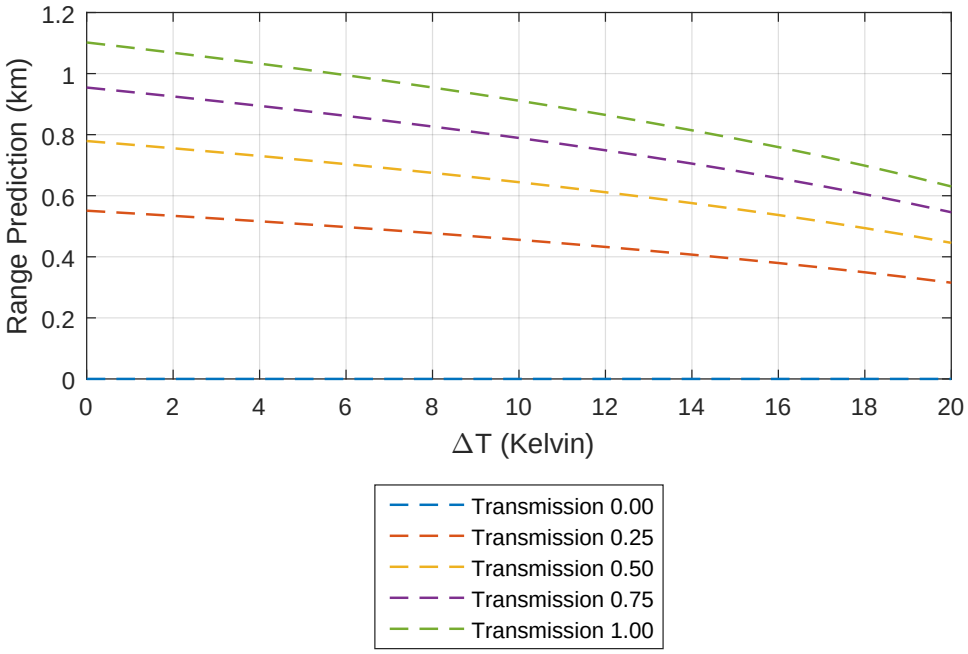

Figure 5.35: Recognition range of land target at LWIR as function of optical transmittance at AC 2

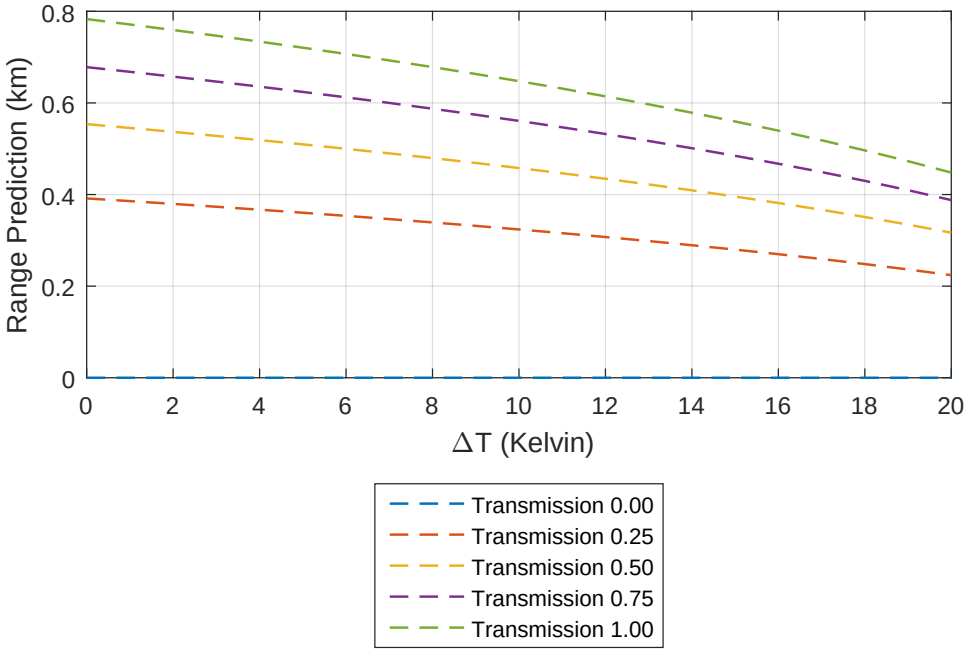

Figure 5.36: Identification range of land target at LWIR as function of optical transmittance at AC 2

Keeping other variables constant, for the land target, results show that the DRI range predictions under the second atmospheric condition increase as the optical transmittance increases. The reason is that the imaging system with optical transmittance naturally collects more radiance. When the value is changed to 1.00 from 0.00, the increase in DRI range prediction is 100% at both band for the land target. For example, the recognition range at MWIR at 0 K ΔT with 0.25 transmittance is 0.37 km, whereas it is 0.75 km for a transmittance value of 1.00. For the LWIR, these values are 0.39 and 0.78 km, respectively.

For the other remaining atmospheric conditions and target types at both bands, once the optical transmittance is changed from 10 to 50 mm, DRI ranges prediction is raised by 400%.

CHAPTER 6

DISCUSSION AND CONCLUSION

In this thesis, radiometry-based range predictions are calculated for three different target types using mid-and long-wave infrared imaging systems. The details of the development of the range prediction equation are presented. The impacts of four different atmospheric conditions on range predictions for both wavelengths are also investigated.

The impacts of the atmospheric transmittance, optical aperture size and transmittance on the range predictions are investigated directly. The impacts of the target area on the range predictions are investigated indirectly, as different target types represent different target areas. Results are presented and results are analyzed in detail in this section.

Chapter 3 presented results of four atmospheric conditions impact on the range predictions for both wavelengths. Furthermore, for each atmospheric condition, the effect of the different target-detector distances on the transmittance is also investigated in this chapter. Results demonstrated that for all the conditions, increasing distance between target and detector decreases the transmittance. At 1 km of target and detector distance, for both wavelengths, the best average transmittance values are obtained, whereas at 20 km the worst average transmittance values are obtained. For example, for the mid wavelength, at the first atmospheric condition, at 1 km of target and detector range, the transmittance is found to be 0.66, whereas at 20 km range, the transmittance decreases to 0.28.

The results also demonstrate that the transmittance for the mid wavelength is higher

than that of for the long-wavelength. Furthermore, mid- and long-wavelength, the best transmittance value is obtained at the first atmospheric condition. Atmospheric transmittance values are very important for the detector manufacturers and infrared imaging system designs. If ignored, the optical design and the detector might not perform well, as the received signal will not be as strong.

Chapter 4 presented the details of the development of the range prediction equation. Detection, recognition, and identification range definitions are also introduced in this chapter.

The results are computed using the developed range prediction equation and chosen required variables in Chapter 5. The impacts of these variables on the range predictions are investigated and presented in this chapter.

Firstly, the impacts of the atmospheric conditions on the range predictions are investigated, keeping all the other variables constant. For mid wavelength infrared imaging system, results demonstrated that the first atmospheric condition give best range predictions for the land target. With respect to the results of the first atmospheric condition, DRI range predictions decreased by 3.11, 18.16, and 52.53% at the second, third, and fourth atmospheric conditions respectively. As it can be interpreted from the results, certain atmospheric conditions impact range predictions significantly more that other atmospheric conditions.

For a land target, up to 14 K target-background temperature difference, ΔT, increasing target temperature decreases DRI range predictions. This trend changes after 14 K ΔT, as increasing target temperature increases range predictions. These results demonstrate that background radiance is dominant up to that threshold. The radiance difference between the target and background is decreasing until 14 K ΔT, and after this threshold, the radiance difference is increasing with increasing target temperature. This is due to the constant background temperature and emissivity, and increasing target temperature. As target temperature increases, the radiance from the target approaches to the background, and then overpasses the background radiance.

This phenomenon does not occur for sea and air targets as the background emissivity significantly lower than that of targets. Because of the constant background tempera-

ture, increasing target temperatures increases DRI range predictions.

When all the other variables kept constant, DRI range predictions are the best at the first atmospheric condition. With respect to the range predictions at this condition, DRI predictions decreases by 3.93, 18.31, and 52.48% at the second, third, and fourth atmospheric conditions respectively for the sea target. Similarly, DRI range predictions decreases by 2.73, 17.79, and 59.50% at the second, third, and fourth atmospheric conditions respectively compared to the DRI range predictions at the first atmospheric condition for the air target.

Similar characters are also observed with the long-wave infrared imaging system as well. Similar to mid-wave study, the land target range predictions have a temperature difference threshold up to where background radiance is dominant; however, this threshold occurs at 20 K for the long-wave imaging system. For the sea target, with respect to the values at the first atmospheric condition, the DRI range predictions decreases by 3.33, 11.77, and 47.10% at the second, third, and fourth atmospheric conditions respectively. The corresponding numbers for the air target are 3.63 , 12.02, and 47.01% respectively.

For mid- and long-wave infrared systems, DRI range predictions decrease as the atmospheric transmittance value decreases. However, although the impact of the atmospheric transmittance on the range predictions is expected to be the same all targets, the observations demonstrate small difference. This is due the random noise fluctuations for the background temperature distribution, which is simulated with MATLAB^{TM} **randn** function.

For a given atmospheric condition and fixed other variables, the effect of the optical aperture size on the DRI range predictions is investigated in detail. Independent of the wavelength of the imaging system, increasing aperture size increases the DRI range predictions as presented in the results section and an example of this situation is shown in Figure 6.1. Similar trends are also observed during the optical transmittance value studies as increasing transmittance increases the DRI range predictions. An example of this situation is shown in Figure 6.2.

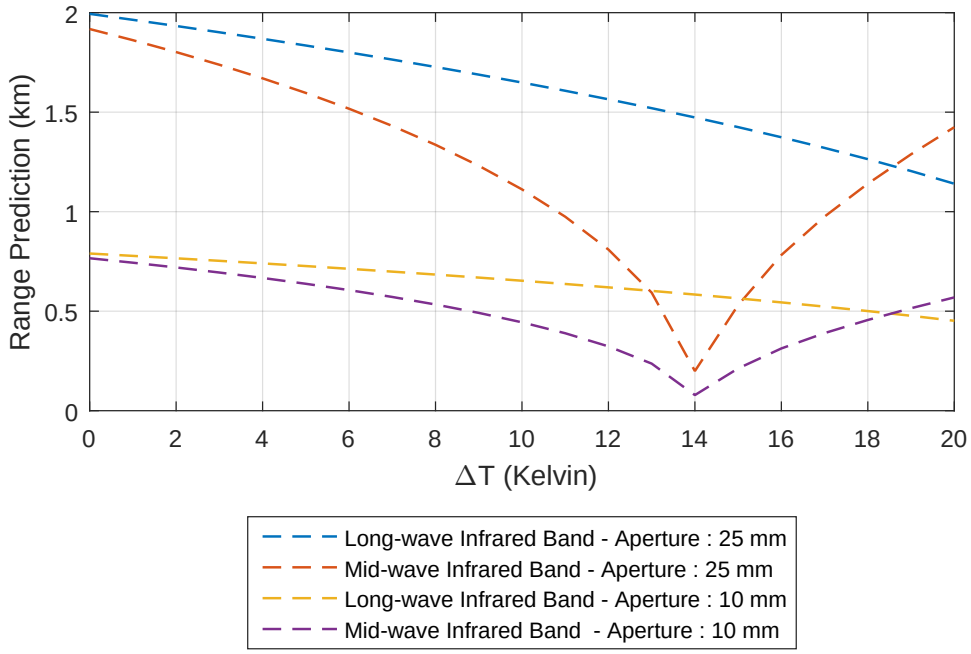

Figure 6.1: Detection ranges of land target for both bands as function of aperture at AC 2

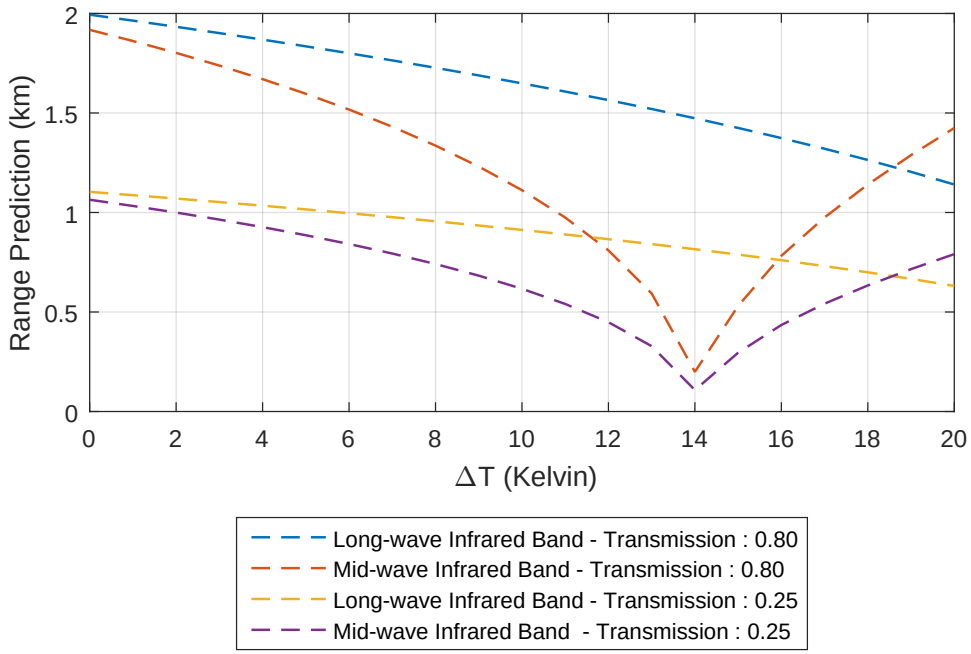

Figure 6.2: Detection ranges of land target for both bands as function of optical transmission at AC 2

Results of this thesis work demonstrate that Long-wave DRI range predictions are better for temperature differences up to 18, 13, and 12 K for the land, sea, and air targets respectively. For temperature differences larger than 18, 13, and 12 K, the mid-wave DRI range predictions are better for those targets. The results of the detection range prediction of land target at both bands under the second atmospheric condition are shown in Figure 6.1 and Figure 6.2 as an example of this situation. These results are observed because long-wave imaging systems receive more radiance at room temperature, whereas mid-wave imaging systems receive more radiance at higher temperatures, as observed in Planck's radiance curves, which is given in Chapter 2.

The target area affects the DRI range predictions. Under normal circumstances, increasing target area increases the DRI range predictions. However, in this thesis work, DRI ranges for an air target with smaller target area are higher than that of an sea target with higher target area due to the fact that the background emissivity values are significantly different for the sea and the air.

In summary, temperature and background emissivity are the two utmost important parameters for radiometer-based range values. In fact, For DRI ranges of a target against the background, it should either have higher-temperature differential or higher emissivity differential or a combination of the both. Therefore, the wavelength choice depends on the different operating scenarios. For scenarios simulated in this thesis work, mid wavelength system performs better for higher target temperatures. Furthermore, for both wavelengths, increasing optical aperture size and transmittance increases DRI range predictions. Similarly, increasing atmospheric transmittance increases DRI range predictions. Results suggest that for range predictions comparison, all the variables have to be taken into account. This work is an early, investigative study. Scenarios simulated in this thesis can be expanded for the optimum design for range.

Following the studies explained in this thesis, it is aimed to test the scenarios discussed here first on hardware in the loop simulation (HWIL) environment and afterwards to test them in real-life. Thanks to these planned follow-up studies, the theoretical studies would be approved by the HWIL and real-life experiments.

REFERENCES

[1] Herschel William (1800). "Experiments on the refrangibility of the invisible rays of the sun" *Philosophical Transactions of the Royal Society of London.*, **90**: 284 - 292.

[2] "Herschel Discovers Infrared Light" *http://coolcosmos.ipac.caltech.edu/cosmic_classroom/classroom_activities/herschel_bio.html*, Retrieved 13.08.2018.

[3] de Saint-Florent (1874) "Photography in natural colours" *The Photographic News*, **18**: 175 - 176.

[4] Herschel, John F.W. (1840). "On chemical action of rays of solar spectrum on preparation of silver and other substances both metallic and nonmetallic and on some photographic processes" *Philosophical Transactions of the Royal Society of London.*, **130**: 1 - 59.

[5] Rajesh Singh Shekhawat. "Infrared Thermography-A Review" *International Journal of Engineering Trends and Technology (IJETT)* , **35**(6): 287 - 290.

[6] Planck, Max (1901). "On the law of energy distribution in the normal spectrum" *Verhandlungen der Deutschen Physikalischen Gesellschaft (in German)*, **2**: 237 - 245. English translation from " The Old Quantum Theory" ed. by D. ter Haar, Pergamon Press, 1967, p.82.

[7] Coblentz, William Weber (1905). "Investigations of Infra-red Spectra: Part I, II" *Carnegie institution of Washington*.

[8] Coblentz, William W. (William Weber) (1905). "Investigations of Infra-red Spectra: Part III, IV" *University of Michigan. Washington, D.C., Carnegie institution of Washington*.

[9] Coblentz, William W. (William Weber) (1905). "Investigations of Infra-red Spectra: Part V, VI, VII" *University of California Libraries. Washington, D.C., Carnegie Institution of Washington.*

[10] Rogalski, Antoni. "History of infrared detectors" *Opto-Electrinocs Review*, **20**(3), 279 - 308.

[11] "Infrared" *https://en.wikipedia.org/wiki/Infrared*, Retrieved 13.08.2018.

[12] Naughton, Russell (2004). "Kalman Tihanyi (1897 - 1947)" *Monash University.*

[13] "Thermographic camera" *https://en.wikipedia.org/wiki/Infrared*, Retrieved 13.08.2018.

[14] "Infrared" *https://en.wikipedia.org/wiki/Infrared*, Retrieved 13.08.2018.

[15] S. Rajkumar and P.V.S.S.R. Chandra Mouli. "Target Detection in Infrared Images Using Block-Based Approach" *Informatics and Communication Technologies for Societal 9 Development*, 2014, 9 - 16.

[16] Mohammad Syuhaimi Ab-Rahman and Mazen R. Hassan "Analytical Analysis of Lock-on Range of Infrared Heat Seeker Missile" *Australian Journal of Basic and Applied Sciences*, **3**(4), 3703 - 3713.

[17] Shahid Baqar. "Low-Cost PC-Based High-Fidelity Infrared Signature Modelling and Simulation" *Cranfield University, Defence College of Management and Technology, Department of Aerospace, Power and Sensors*, Chapter 6, July 2017.

[18] Monroe Schlessinger. "Infrared Technology Fundamentals" *M. Dekker Inc.*, New York, 1995.

[19] Richard D Hudson. "Infrared System Engineering" *Wiley-Interscience*, New York, 1969.

[20] Arnold Daniels. "Field Guide to Infrared Systems" *SPIE-The International Society for Optical Engineering*, Bellingham, 2007.

[21] Arnold Daniels. "Field Guide to Infrared Systems, Detectors, and FPAs" *SPIE-The International Society for Optical Engineering*, Bellingham, 2007.

[22] Sean J. Kirkpatrick. "A primer on radiometry" *Dental Materials, Elsevier*, 2005 (21)(1), 21 - 26

[23] Ronald G. Driggers, Paul Cox and Tim Othy Edwards. "Introduction to Infrared and Electro-Optics systems" *Artech House*, London, 1999.

[24] George J Zissis and Joseph S. Accetta. "The Infrared and Electro-Optical Systems Hand book, Volume-1: Sources of Radiation" *SPIE Optical Engineering Press*, Washington USA, 1993.

[25] Alexander Berk, Gail P. Anderson and Brett Gossage. "MODTRAN 5.3.2 User's Manual" *Spectral Sciences, Inc., Air Force Research Laboratory*, May 2013.

[26] "Turkish Armed Force" *https://www.flickr.com/photos/131986175@N03/*, Retrieved 13.08.2018.

[27] Gerald C. Holst. "Electro-Optical Imaging System Performance" *JCD Publishing, SPIE*, 2000.

[28] Aparna Akula, Ripul Ghosh, H K Sardana "Thermal Imaging And Its Application In Defence Systems" *Optics: Phenomena, Materials, Devices, and Characterization AIP Conf. Proc. 1391, 333 - 335*, 2011

[29] Robert S. McDonald "Review: Infrared Spectrometry" *Analytical Chemistry vol. 58, no. 9, 1906 - 1925*, 1986

[30] A. Rogalski "History of infrared detectors" *Opto - Electronics Review 20(3), 279 - 308*, 2012

[31] Shripad P. Mahulikar , Hemant R. Sonawane, G. Arvind Rao "Infrared signature studies of aerospace vehicles" *Progress in Aerospace Sciences, Elsevier Volume 43 Issues 7-8, 218 - 245*, 2007

[32] B. T. Barnes, W. E. Forsythe, and E. Q Adams "The Total Emissivity of Various Materials at 100-500 C" *Journal of the Optical Society of America Volume 37 Number 10, 804 - 806*, 1947

[33] Masanori Konda, Norihisa Imasato, Katsu Nishi and Takashi Toda "Measurement of the Sea Surface Emissivity" *Journal of Oceanograph Vol.50, pp. 17 - 30*, 1994

[34] Oved Naveh "Sensitivity of scanning and staring infrared seekers for air-to-air missiles" *Proc. SPIE 3061, Infrared Technology and Applications XXIII*, 1997

[35] Berk Berkan Turgut, Goktug Gencehan Artan, Alpan Bek "A comparison of MWIR and LWIR imaging systems with regard to range performance" *Proceedings Volume 10625, Infrared Imaging Systems: Design, Analysis, Modeling, and Testing XXIX; 1062512*, 2018

APPENDIX A

MATLAB™ GUI PROGRAM

In this thesis, graphical interface program for range prediction with using the MATLAB 2015A® is prepared. The interfaces of program is given in Figures A.1, A.2, and A.3. Welcome section is shown in Figure A.1. Particular parameters section which is shown in Figure A.2 are required to compute the range prediction. And last section is an output section which is given Figure A.3.

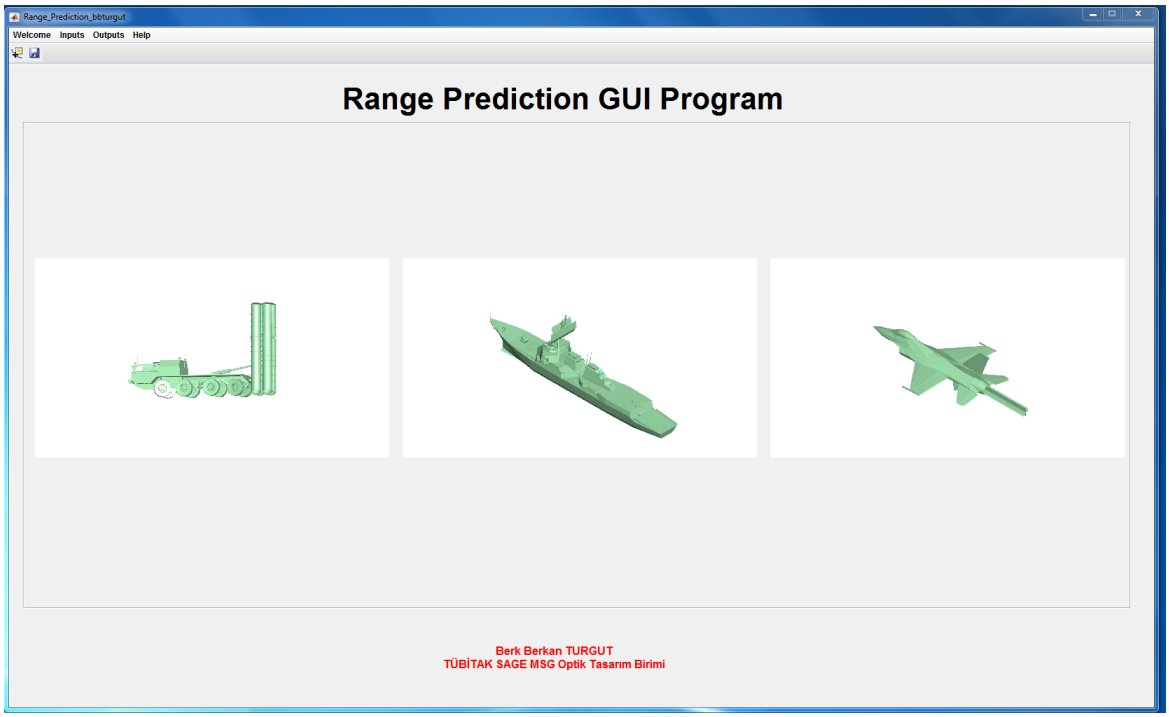

Figure A.1: MATLAB GUI 1

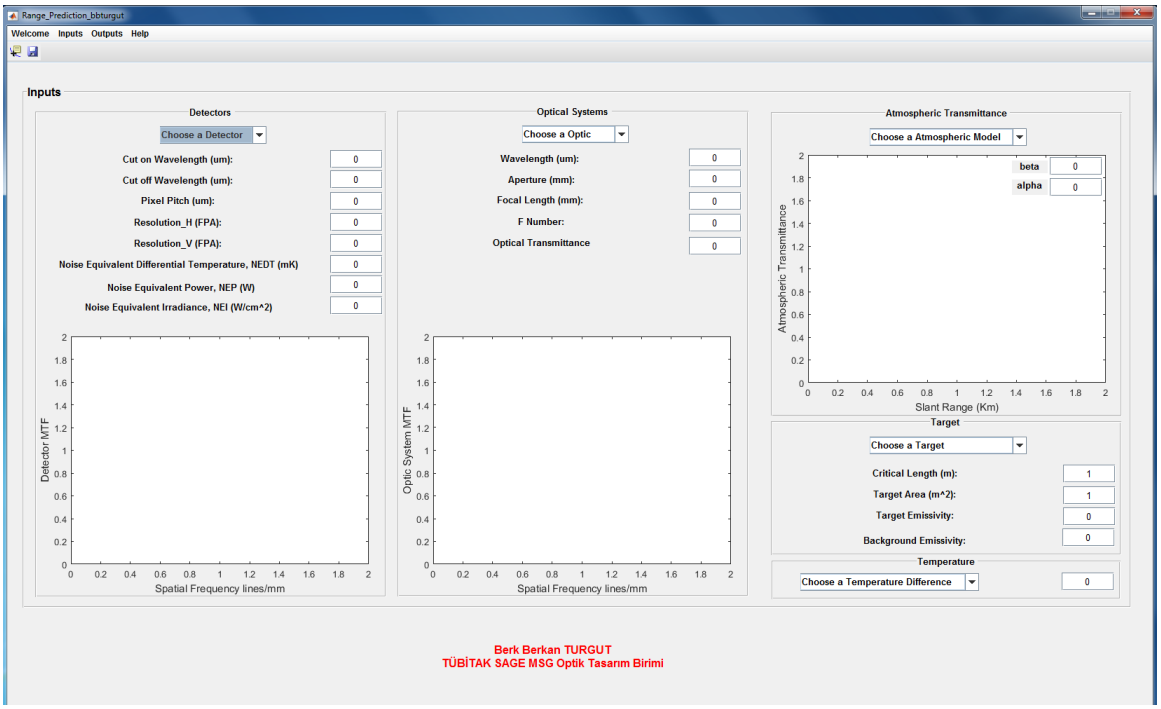

Figure A.2: MATLAB GUI 2

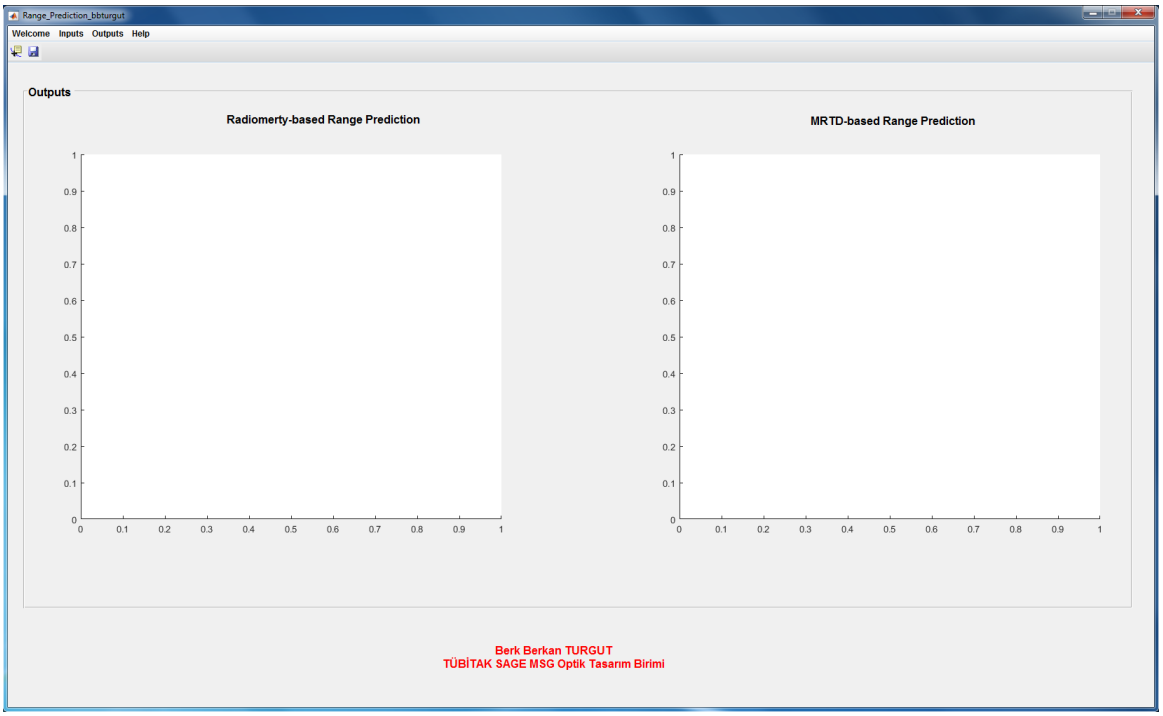

Figure A.3: MATLAB GUI 3

APPENDIX B

MODTRAN™ PROGRAM

In this thesis, MODTRAN5® software is used to compute the atmospheric transmittance at various atmospheric conditions for MWIR and LWIR imaging systems. The interfaces of the software are given in Figure B.1, B.2, B.3, and B.4. The parameters of atmosphere are chosen using atmosphere tab which is demonstrated in Figure B.1 and B.2. For the aerosol model, aerosol tab is used as illustrated in Figure B.3. Finally, the scenario is determined to calculate the atmospheric transmittance. The geometry tab is used for this purpose and that tab is shown in Figure B.4.

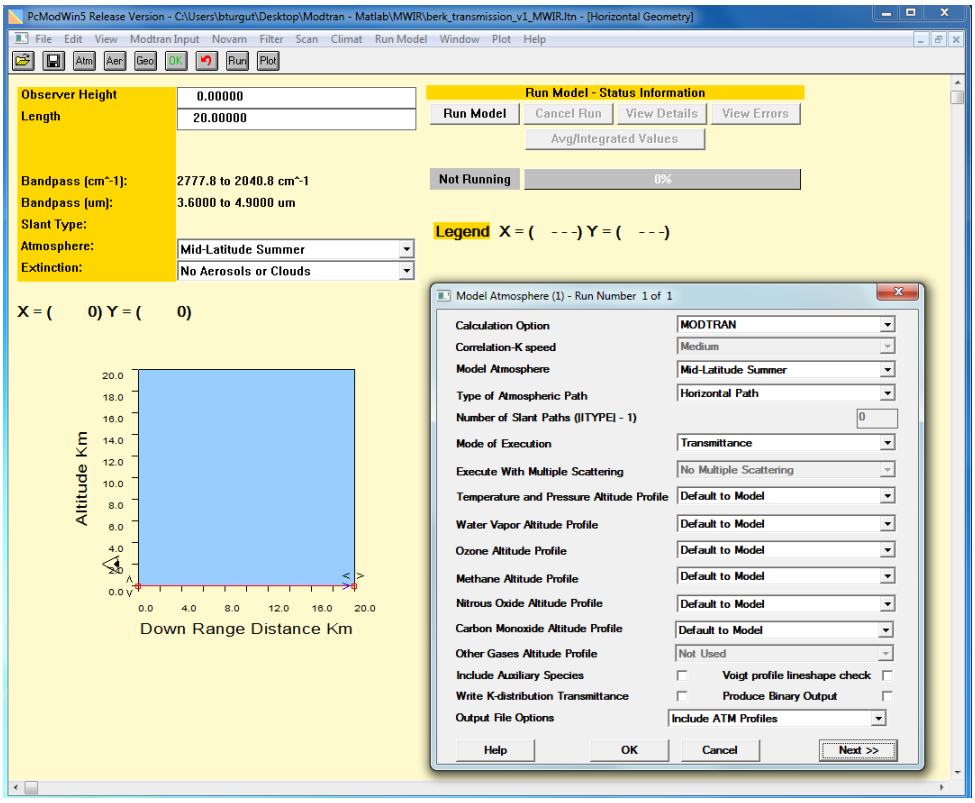

Figure B.1: MODTRAN interface 1

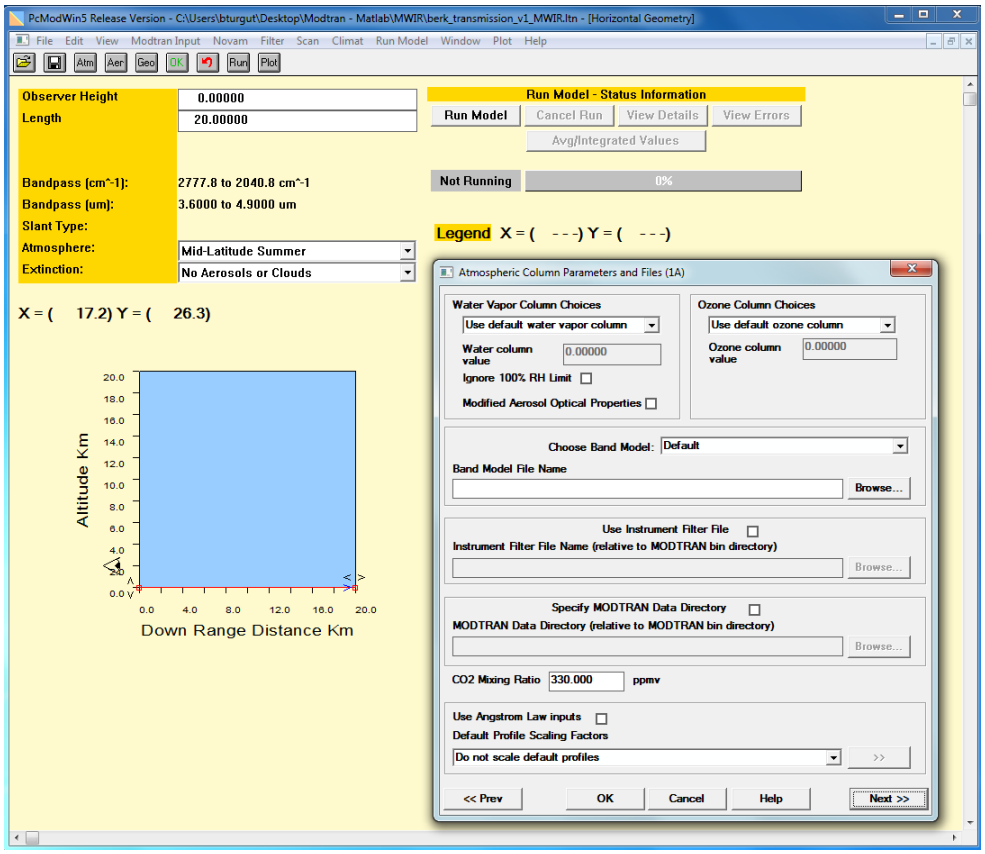

Figure B.2: MODTRAN interface 2

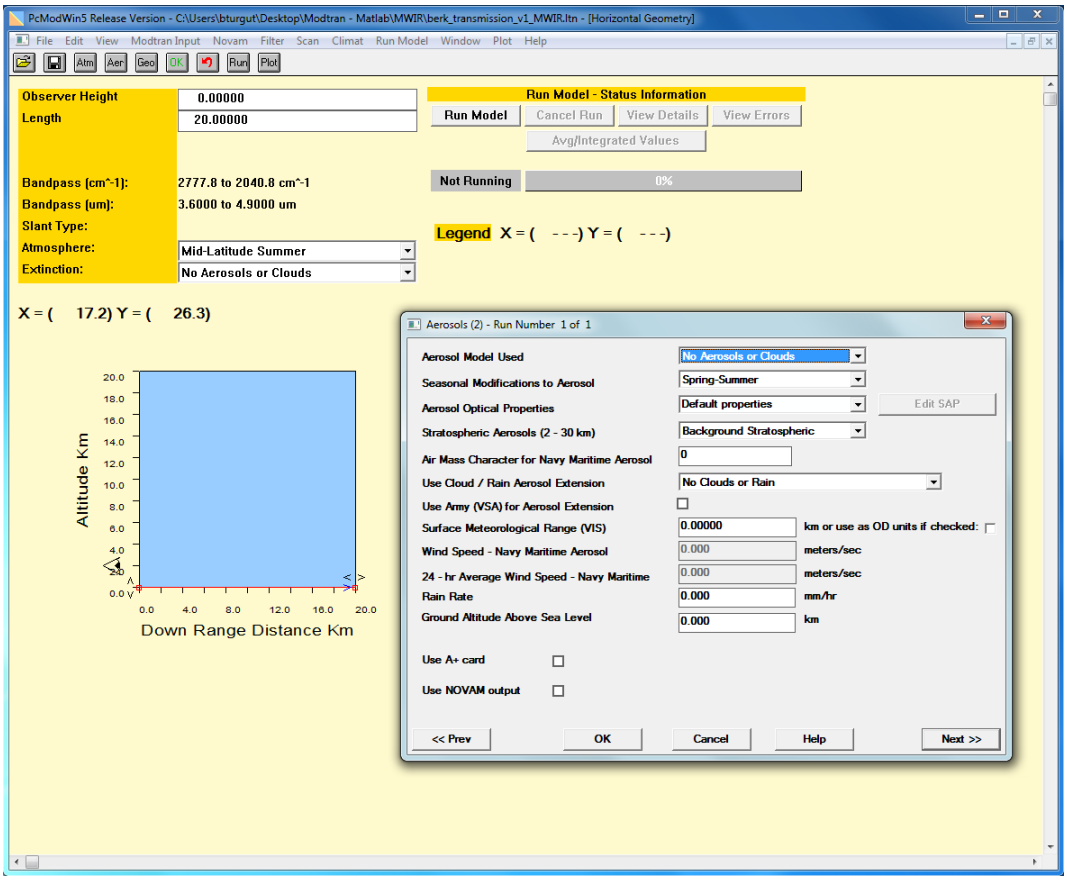

Figure B.3: MODTRAN interface 3

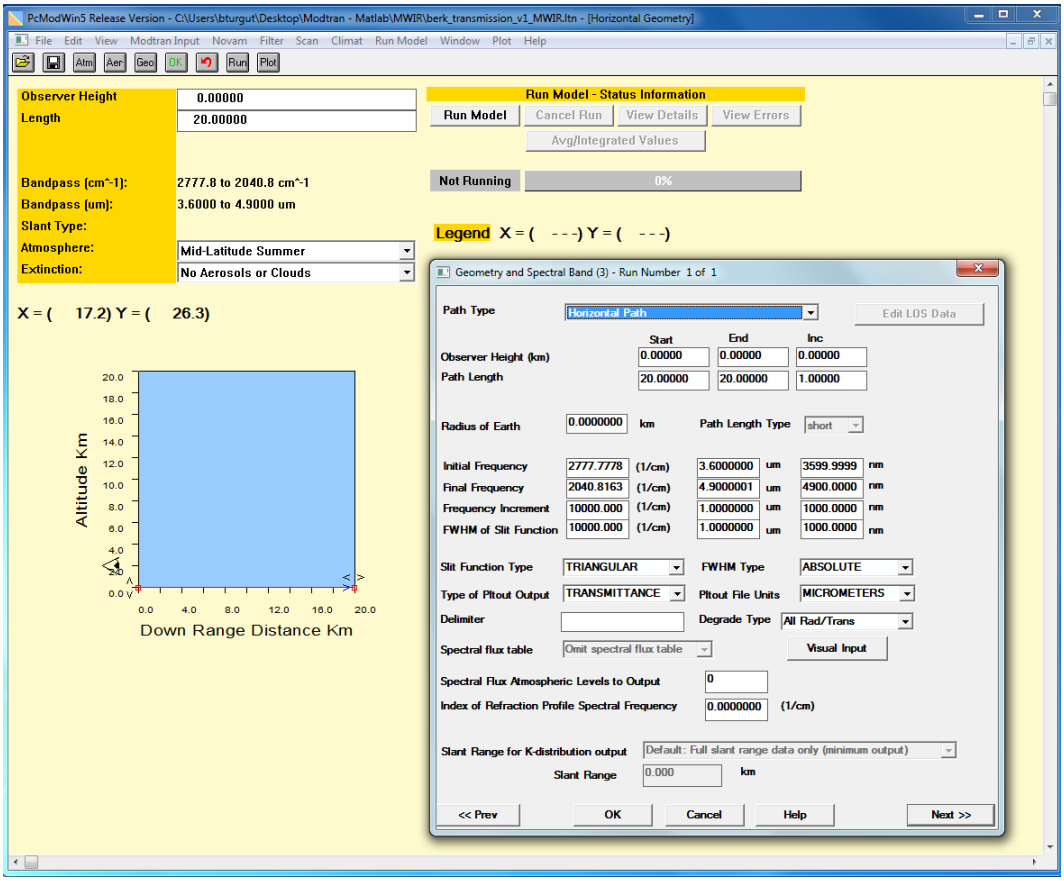

Figure B.4: MODTRAN interface 4